Journal Pre-proof

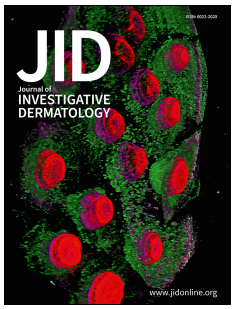

Somatic loss-of-function *PIK3R1* and activating non-hotspot *PIK3CA* mutations associated with Capillary Malformation with Dilated Veins (CMDV)

Martina De Bortoli, MSc, Angela Queisser, PhD, Van Cuong Pham, MSc, Anne Dompmartin, MD, PhD, Raphaël Helaers, PhD, Simon Boutry, MSc, Cathy Claus, MD, PhD, An-Katrien De Roo, MD, Frank Hammer, MD, Pascal Brouillard, PhD, Salim Abdelilah-Seyfried, PhD, Laurence M. Boon, MD, PhD, Miikka Vikkula, MD, PhD

PII: S0022-202X(24)00164-7

DOI: https://doi.org/10.1016/j.jid.2024.01.033

Reference: JID 4180

To appear in: *The Journal of Investigative Dermatology*

Received Date: 18 September 2023

Revised Date: 25 January 2024

Accepted Date: 27 January 2024

Please cite this article as: De Bortoli M, Queisser A, Pham VC, Dompmartin A, Helaers R, Boutry S, Claus C, De Roo A-K, Hammer F, Brouillard P, Abdelilah-Seyfried S, Boon LM, Vikkula M, Somatic loss-of-function *PIK3R1* and activating non-hotspot *PIK3CA* mutations associated with Capillary Malformation with Dilated Veins (CMDV), *The Journal of Investigative Dermatology* (2024), doi: https://doi.org/10.1016/j.jid.2024.01.033.

Somatic loss-of-function *PIK3R1* and activating non-hotspot *PIK3CA* mutations associated with Capillary Malformation with Dilated Veins (CMDV)

Martina De Bortoli, MSc, [1] ORCID: 0009-0002-2455-1731 (Twitter (X): @DbortoliMartina)

Angela Queisser, PhD, [1] ORCID: 0000-0002-0993-9132 (Twitter (X): @queisserangela)

Van Cuong Pham, MSc, [2] ORCID: 0000-0003-4787-7013

Anne Dompmartin, MD, PhD, [3] ORCID: 0000-0003-0081-500X

Raphaël Helaers, PhD, [1] ORCID: 0000-0002-7046-7867

Simon Boutry, MSc,[1, 4] ORCID: 0000-0002-3214-2981 (Twitter (X): @BoutrySimon)

Cathy Claus, MD, PhD,[5] ORCID: 0009-0005-7560-7020

An-Katrien De Roo, MD, [5, 7, 8] ORCID: 0000-0002-0000-1260

Frank Hammer, MD, [9] ORCID: 0000-0003-0745-3830

Pascal Brouillard, PhD,[1] ORCID: 0000-0001-9548-8229 (Twitter (X): @Pasc_Brouillard)

Salim Abdelilah-Seyfried, PhD,[2] ORCID 0000-0003-3183-3841

Laurence M. Boon, MD, PhD, [1,5] ORCID: 0000-0001-8273-3328 (Twitter (X): @LaurenceBoon4)

Miikka Vikkula, MD, PhD, [1, 5, 6] ORCID: 0000-0002-6236-338X (Twitter (X): @MiikkaVikkula)

1. Human Molecular Genetics, de Duve Institute, UCLouvain, Brussels, Belgium.
2. Institute of Biochemistry and Biology, Potsdam University, Potsdam, Germany.
3. Department of Dermatology, Université de Caen Basse Normandie, CHU Caen, Caen, France.
4. Interuniversity Institute of Bioinformatics in Brussels, Université Libre de Bruxelles-Vrije Universiteit Brussel, 1050 Brussels, Belgium.

5. Center for Vascular Anomalies, Division of Pathology, University Clinics Saint-Luc, UCLouvain, Brussels, Belgium; VASCERN VASCA European Reference Centre
6. WELBIO department, WEL Research Institute, avenue Pasteur, 6, 1300 Wavre, Belgium.
7. Service d'anatomopathologie, Cliniques Universitaires Saint-Luc, 10, avenue Hippocrate, 1200 Bruxelles, Belgique
8. Institute of Experimental and Clinical Research, UCLouvain, Avenue Hippocrate 55 box B1.55.02, 1200 Brussels, Belgium.
9. Department of Medical Imaging, Cliniques Universitaires Saint-Luc, UCLouvain, Brussels, Belgium

Corresponding Author:

Miikka Vikkula, MD, PhD

Human Molecular Genetics

de Duve Institute, University of Louvain

Avenue Hippocrate 74 (+5), bte B1.74.06

B-1200 Brussels, Belgium

phone/secretary: + 32-2-764 7490

fax: + 32-2-764 7460

miikka.vikkula@uclouvain.be

Keywords:

PI3K signaling, NGS, somatic, endothelial, zebrafish

ABSTRACT

Common capillary malformations (CMs) are red vascular skin lesions, most commonly associated with somatic activating *GNAQ* or *GNA11* mutations. We focused on CMs lacking such a mutation to identify novel genetic causes. We used targeted next-generation-sequencing on 82 lesions. Bioinformatic analysis allowed the identification of 9 somatic pathogenic variants in *PIK3R1* and *PIK3CA*, encoding for the regulatory and catalytic subunits of the PI3K kinase, respectively. Re-characterization of these lesions unraveled a common phenotype: a pale Capillary Malformation associated with visible Dilated Veins (CMDV). Primary-endothelial cells from two *PIK3R1*-mutated lesions were isolated and PI3K-AKT-mTOR and RAS-RAF-MAPK signaling were assessed by western-blot. This unveiled an abnormal increase in AKT phosphorylation, effectively reduced by PI3K pathway inhibitors, such as mTOR, AKT and PIK3CA-inhibitors. The effects of mutant *PIK3R1* were further studied using zebrafish embryos. Endothelium-specific expression of *PIK3R1* mutants resulted in abnormal development of the posterior capillary-venous plexus. In summary, CMDV emerges as a clinical entity associated with somatic pathogenic variants in *PIK3R1* or *PIK3CA* (non-hotspot). Our findings suggest that the activated AKT signaling can be effectively reversed by PI3K-pathway inhibitors. Additionally, the proposed zebrafish model, holds promise as a valuable tool for future drug screening aimed at developing patient-tailored treatments.

INTRODUCTION

Capillary Malformations (CM), commonly known as "port-wine stains", are usually unifocal lesions, affecting mainly the skin or mucosa in localized areas. CMs usually appear sporadically as red or purple flat macules. They are the most common cutaneous vascular malformation, affecting around 3/1000 newborns (Uebelhoer et al., 2012; Walton et al., 1976). Most of the sporadic cases (around 90%) of common CM have been associated with an activating somatic mutation in the *GNAQ* or *GNA11* gene (Couto et al., 2016; Nakashima et al., 2014). Less common capillary phenotypes also exist: 1) more extensive CM, such as CM with overgrowth (CMO) or diffuse CM with proportionate overgrowth (DCMO), 2) multifocal CMs, such as in CM associated with arteriovenous malformations (CM-AVM1 and CM-AVM2), and 3) combined lesions, such as capillaro-lymphatico-venous malformation (CLVM) and capillary-venous malformations (CVM, (Uihlein et al., 2013)) with or without overgrowth. Some CMO and DCMO have been shown to associate with somatic *GNAQ* or *PIK3CA* non-hot spot mutations, respectively (Goss et al., 2020; Jordan et al., 2020), whereas CM-AVM1 and 2 are associated with germline *RASA1* and *EPHB4* mutations (Amyere et al., 2017; Eerola et al., 2003). Many of the patients with combined lesions bear a somatic activating *PIK3CA* hotspot mutation (Brouillard et al., 2021; Keppler-Noreuil et al., 2016). Nonetheless, numerous CM lesions remain unsolved, without detection of such a mutation.

To date, gold-standard treatments for vascular malformations include laser, sclerotherapy, embolization and surgical resection. Since the discovery of the underlying signaling pathways that are shared with cancers, oncology drugs have been tested in preclinical models of vascular malformations and also in clinical trials (Adams et al., 2016; Boon et al., 2022; Boscolo et al., 2015; Harbers et al., 2023; Queisser et al., 2021; Seront et al., 2023). These drugs have demonstrated their effectiveness in vascular anomalies (VA) patients, and they will likely be

selected based on patients' genotypes. Therefore, it has become crucial to identify all the genes and mutations that can lead to vascular anomalies.

We have sequenced DNA from resected lesions and from patient-derived endothelial cells (EC) from a cohort of individuals affected by sporadically occurring CM. No mutation in *GNAQ* or *GNA11* had been detected and other genes were analyzed. We describe somatic mutations in two genes belonging to the PI3K/AKT/mTOR pathway, observe activation of this pathway and their response to drug treatment in isolated ECs, and show a zebrafish model we generated for one of the genes. Our clinical re-evaluation of the patients revealed lesions with characteristics that differ from those of common CM: a pale CM with visible dilated veins. This entity has been reported in the literature as CVM (Uihlein et al., 2013). Here we propose a diagnostic term that more precisely describes the clinical characteristics, as we do not observe a proper venous malformation (VM) in these lesions.

RESULTS

***PIK3R1* and *PIK3CA* somatic variants found in nine patients**

We identified *PIK3R1* (NM_181523.2) or *PIK3CA* (NM_006218.2) somatic variants in the lesions resected from nine individuals **(Table 1)**. Four were distinct variants in *PIK3R1* and three in *PIK3CA,* from 5 and 4 patients, respectively **(Figure 1 and Table 1)**. All the identified variants in *PIK3R1* and *PIK3CA* are predicted to be damaging by at least 11 prediction algorithms and reported in the COSMIC database for cancer somatic mutations. Three out of the four *PIK3R1* variants (G376R, N564D, L573P) are among the twenty most recurrent *PIK3R1* variants on a total of 1663 observed in cancers **(Table 1)**, whereas the three variants in *PIK3CA* are not the canonical hotspots **(Figure 1B in grey)**. The variant allele fraction (VAF) ranged from 3% to 18%, reflecting somatic etiology **(Table 1)**. The four *PIK3R1* variants were missense changes located in the nSH2 (n=1) or the PI3K_p85_iSH2 (n=3, accounting for 4

patients) domains of the p85 protein **(Figure 1A**). These domains interact with the catalytic p110 subunits of the PI3K kinase. The three distinct missense changes in *PIK3CA* were located in the C2 domain (n=2, accounting for 3 patients) or in the PI3K catalytic domain of the p110 protein (n=1) **(Figure 1B)**. To date, on the total of 82 screened individuals, 61 still remain "unsolved".

Patients harboring *PIK3CA* and *PIK3R1* variants have a distinct clinical entity

Following identification of the genetic variants, the clinical re-evaluation noted similarities between the lesions. The lesion size varied from small patches to more extensive ones. They manifested as red to dark-red lesions at birth, with indistinct borders, becoming paler and more purple-colored over time **(Figure 2C)**. They also had visible dilated veins along with the capillary malformation irrespective of the body part they were localized in **(Figure 2)**.

Seven of the nine patients had a lesion localized on the lower extremities (Patients 1-6 and 9) **(Figure 2)**. Patient 7 had a lesion on the upper extremity (from hand to axilla), while patient 8 had a lesion on the right lower flank only. Two of the patients with a lower extremity lesion had an extensive CMDV: patient 9 had a lesion on the entire left lower extremity with varicose veins in the genitalia, and patient 2 had bilateral lesions extending to the lower back. The other lower extremity lesions affected only partially the limb **(Figure 2)**.

Doppler Ultrasound and MRI showed dilation of the superficial, muscular and sometimes deep veins without aplasia or hypoplasia of the deep venous system or persistent embryonic veins **(Figure 2D)**. D-dimers levels were in the physiological range for all patients, except for Individual 2 in which they were found to be slightly increased during sporadic episodes of pain. Some patients had mild hypo or hypertrophy of soft tissue or bone with larger or smaller girth and/or longer or shorter leg (n=4) **(Table 2)**. There were no foot or toe anomalies. Patients reported pain at the site of the dilated veins, mostly mild, with episodes of stronger pain (n=3).

Only one patient reported functional limitations due to pain (Individual 1). None of the patients displayed signs of overgrowth or lymphatic malformations. Treatment of these patients is now limited to pain management, when necessary, and treatment of dilated veins using surgical or sclerotherapeutical approaches.

Patient-derived ECs with a *PIK3R1* mutation show activation of PI3K-AKT-mTOR and RAS-RAF-MAPK pathways.

Primary-ECs derived from surgical resections of two *PIK3R1*-positive lesions were isolated from non-endothelial cells. $CD31^+$ cells displayed the cobblestone morphology typically seen for ECs, whereas $CD31^-$ cells appeared more elongated **(Figure 3A)**. The isolated ECs expressed CD31 (in red) and a second EC marker, von Willebrand factor (vWF, in green) **(Figure 3B)**.

To confirm the presence of the *PIK3R1* mutation and to define VAF, DNA of the patient-derived endothelial cells were sequenced by targeted-NGS. One EC bore the same c.1690A>G (N564D) variant as the corresponding tissue sample (Tissue 7 – **Table 1 and 2**), while the other harbored the same c.1718T>C (L573P) *PIK3R1* variant as the corresponding tissue sample (Tissue 9 – **Table 1 and 2**). From this point forward they will be referred as EC-N564D and EC-L573P. Both $CD31^+$ cells had a VAF around 50%. In $CD31^-$ cells, no *PIK3R1* variant was detected.

To assess if the *PIK3R1* variants could trigger activation of the PIK3-AKT-mTOR or the RAS-RAF-MAPK pathway in the mutant ECs, we measured the levels of pAKT and pERK. Compared to HUVECs, AKT phosphorylation was increased in both EC-N564D and EC-L573P, as well as in control ECs expressing *PIK3CA*-hotspot mutation (**Figure 4A, 4B**). In addition, EC-N564D grown under starved conditions induced higher levels of pAKT compared to HUVECs **(Figure 4A, 4B)**. ERK-phosphorylation was observed when EC-N564D were

grown in complete medium, as well as in starved conditions **(Figure 4C)**. pERK levels were also higher in EC-L573P compared to HUVECs **(Figure 4D)**.

PI3K-AKT-mTOR and RAS-RAF-MAPK pathways effectively inhibited in *PIK3R1* mutant ECs

Patient-derived ECs were treated with inhibitors acting at different levels of the PIK3-AKT-mTOR signaling pathway: the mTOR-inhibitor rapamycin (Sirolimus), the AKT-inhibitor MK2206 and the PIK3CA-inhibitor BYL719 (Alpelisib). Treatment of EC-N564D and EC-L573P resulted in a significant decrease in pAKT **(Figure 4A, 4B)**. The reduction was particularly striking when MK2209 and BYL719 were used. A decrease in pERK was also observed, but this was limited to the treatment with the PIK3CA inhibitor BYL719 **(Figure 4C, 4D)**. Of note, the experiments were only performed twice for EC-L573P, as the piece of tissue harvested during surgical procedure was small and the number of passages that were obtained for the limited number of ECs was low before they ceased to grow.

Endothelium-specific expression of mutant *PIK3R1* in zebrafish embryos leads to malformations in the capillary-venous network

To further assess the effects of the CMDV-PIK3R1 variants, we generated zebrafish models. We first performed a knock-down experiment in Tg*(fli1a:Gal4FF^{ubs3};UAS:RFP)* embryos, by injecting a spliced *PIK3R1* morpholino at one-cell stage, in order to evaluate the overall effect of *PIK3R1* loss. Compared to uninjected embryos, the diameter of the caudal vein (CV) was significantly increased **(Figure S1A)**.

Additionally, we performed endothelium-specific mosaic overexpression of the WT/mutant *PIK3R1* transgene in zebrafish. Upon overexpression of *PIK3R1*^{N564D}, *PIK3R1*^{L570P} and *PIK3R1*^{L573P} mutations in these embryos, the CP appeared mostly disorganized, showing

an irregular, compressed morphology with indistinguishable individual vessels, rather than an organized pattern of small, connected vessels **(Figure 5A-F)**. This phenotype was more objectively measured by spatial analysis of the vascular area by calculating the ratio between the intravascular and intervascular spaces within the capillary bed, which corroborated our initial visual observation **(Figure 5G)**.

Moreover, overexpression of *PIK3R1*^{L570P} and *PIK3R1*^{L573P}, but not of *PIK3R1*^{N564D}, led to enlargement of the CV diameter **(Figure 5A-F, 5H)**. Neither morphants nor mutant fish exhibited any indication of developmental delay **(Figure S2)**. Embryos in which the CV was not readily distinguishable were omitted from the analysis. This was more frequent for mutant embryos, than for control or WT embryos **(Table S1)**. This trend is particularly pronounced in PIK3R1^{N564D} , PIK3R1$^{N564D+pik3r1Mo}$ and PIK3R1^{L573P} mutants, in which the percentage of discarded embryos reached 42,8%, 33,33% and 30,7% respectively **(Table S1)**.

To assess whether WT or mutant *PIK3R1* could rescue the phenotype induced by the morpholino, knocked-down embryos were injected along with the corresponding plasmids. We found that the vascular phenotype was solely attributable to the gene knockdown. In fact, neither the mutant nor WT *PIK3R1* mosaic re-expression had the capacity to rescue the CV phenotype, nor did it induce any additional phenotypic changes **(Figure S1B, S1C, S1D)**. No variant-specific additional phenotypes were observed. The rate of plasmid integration was estimated by counting the number of EGFP+ ECs in the zebrafish trunk, specifically in the area between the dorsal aorta (DA) and the CV (**Figure 5I**; **Figure S1E)**. This method provided an indication of the degree of mosaicism in the mutant fish and suggested that control embryos (EV and EV + *pik3r1Mo*) had a higher integration rate compared to those injected with *PIK3R1*, with the exception of the *PIK3R1*^{L570P} mutant.

DISCUSSION

In this study we describe a CM subtype, CMDV, which we found to be associated with somatic mutations in two genes belonging to the PI3K-AKT-mTOR signalling pathway: *PIK3R1* and *PIK3CA* **(Figure 6).**

In patients, the clinical phenotype primarily manifests as a common, small CM on the limbs. These CM exhibit pale, purplish indistinct borders, which stand in contrast to the well-defined reddish borders typically observed in "classic" CM cases. Patients had no or limited hypertrophy of soft tissues, yet they exhibit prominent dilated cutaneous veins on the CM. Neither overgrowth, nor signs of skeletal or lymphatic malformation were observed. Likely, many of these patients are now misdiagnosed as mild Klippel Trenaunay syndrome (KTS), lacking a lymphatic component. Our patient cohort, on the other hand, exhibited mild to no pain, normal levels of D-dimers, no involvement of the deep venous system, and, therefore, no increased risk of thromboembolism. These characteristics serve to further differentiate them from individuals with KTS. Such lesions were described earlier and recognized as Capillary Venous Malformations (CVM) (Uihlein et al., 2013). To emphasize the predominant clinical feature – namely, a CM accompanied by dilated veins – we propose to rename them "*Capillary Malformation with Dilated Veins*" (CMDV). Following the recently proposed gene-phenotype based nomenclature (Biesecker et al., 2021), we suggest calling the CMDV lesions when genetic data is available, PIK3R1-CMDV and PIK3CA-CMDV.

The four somatic variants identified in *PIK3R1* are known in cancer (Chen et al., 2018; Jaiswal et al., 2009). Typically, they are oncogenic mutations that disrupt the inhibitory activity of p85 on the p110-catalytic subunit, while maintaining the stabilizing effect, resulting in p110-mediated activation of downstream signaling pathways (Jaiswal et al., 2009). While the G376R and N564D variants have been characterized *in vitro* (Jaiswal et al., 2009; Li et al., 2021), the

L570P and L573P variants are predicted to be pathogenic, but lack experimental validation. PIK3R1 mutations have only recently been reported in vascular malformations, within the context of *PIK3R1*-related overgrowth syndromes that mimic *PIK3CA*-related overgrowth syndromes (PROS) (Cottrell et al., 2021; Siegel et al., 2018).

The three variants identified in *PIK3CA* are missense somatic "non-hotspot" variants (allele frequency 3-7%) localized in the C2 domain (involved in binding to the phospholipid membrane) and in the PI3K catalytic domain. Two of the three variants (E453K and M1043I) enhance transformation of Ba/F3 cells and induce AKT phosphorylation (Dogruluk et al., 2015; Gymnopoulos et al., 2007; Jin et al., 2021; Ng et al., 2018). This activation is weaker than that induced by the E542/545K and H1047R hotspots. Yet, this indicates that these non-hotspot variants provide driver activity. The C378Y variant remains uncharacterized.

Somatic *PIK3R1* mutations were reported in a series of 12 individuals with vascular malformations. The authors had included patients with a PROS-like phenotype, consisting of capillary, venous and lymphatic malformations, lipoma/fatty tissue overgrowth and digital abnormalities, making it clinically difficult to distinguish them from those with a PROS due to a somatic *PIK3CA* mutation (Cottrell et al., 2021). In addition, a somewhat similar cutaneous phenotype to CMDV has also been recently associated with severe focal cortical dysplasia and a variant in the *AKT3* gene (De Bortoli et al., 2024).

As the clinical and genetic spectrum of vascular anomalies continues to be defined, the clinic-genetic distinctions are becoming increasingly important. Precision therapies continue to be developed and organotypic vessel types are acknowledged (Petrova and Koh, 2018). Thus, anomalies due to different genes and even variants in the same gene, and the different vessel types they affect in a given lesion, may respond differently to therapeutic approaches.

Sequencing of primary ECs derived from two PIK3R1-CMDV patients revealed a mutant allele frequency of approximately 50%, in contrast with the lower somatic percentages detected

in the corresponding tissue samples. This indicates that all the isolated ECs were likely heterozygous for the somatic mutation. This could be due to their better survival or high frequency of mutant ECs in the patients' resected tissue. Anyhow, the somatic mutation was not detected in the non-ECs, confirming that the source of the malformation resides within the vascular endothelium.

The *PIK3R1* c.1690A>G; N564D has previously been demonstrated to promote p110-independent cell survival, increased AKT signaling and anchorage-independent growth of epithelial and Ba/F3 cells (Jaiswal et al., 2009; Urick et al., 2011) as well as epithelial cell proliferation in the absence of EGF (Chen et al., 2018). To assess whether this also happens in CMDV and in primary cells, we characterized the *PIK3R1* L573P and N564D variants in patient-derived ECs. We showed an increase in pAKT and pERK, even when CMDV-ECs were grown in starved conditions. This suggests that the downstream cell-survival and proliferation pathways are activated as a direct consequence of the mutations, and this is not dependent on growth factors. However, AKT-phosphorylation was weaker in EC-N564D and EC-L573P compared to PIK3CA-hotspot-CLVM cells, underscoring the clinical distinction between the milder PIK3R1-CMDV and the more severe PIK3CA-hotspot manifestations.

Treatment of EC-N564D and EC-L573P with PI3K-pathway inhibitors (sirolimus, MK2206 and BYL719) **(Figure 4)** significantly reduced pAKT levels, confirming the potential of pre-existing cancer drug for treating CMDV. In EC-N564D, pERK levels were not decreased by the mTOR and AKT-inhibitors, as these targets are not part of the MAPK pathway. However, we found BYL719 to be very effective in reducing pERK levels. This suggests that a cross-talk between PI3K and MAPK pathways could take place at the level of PI3K, right after the binding of the ligand to the RTK and the activation of the cytosolic kinases. Altogether, these data suggest that *PIK3R1* mutations in ECs are sufficient to trigger the activation of the

PI3K and MAPK pathways, and the inhibition of the upstream PI3K kinase is enough to block both cascades.

Zebrafish has already been used to model vascular malformations (Al-Olabi et al., 2018; Bell et al., 2021). We thus next employed it to replicate CMDV manifestations *in vivo*. Endothelium-specific mosaic embryos that exclusively expressed the transgene in the vasculature allowed us to mimic the conditions of mosaic CMDV patients. Two main phenotypes, recapitulating the CMDV patients' manifestations, were observed in mutant embryos: (i) enlargement of the CV diameter and (ii) disruption of the capillary network.

Specifically, enlarged CV occurred only in cases of complete *PIK3R1* knockdown as well as upon overexpression of two-out-of-three mutant *PIK3R1*, suggesting these variants to be LoF. We attribute the lack of statistical significance for the PIK3R1^{N564D} variant to the substantial variability in the mosaicism levels among embryos. Assessment of cell size, based on measurements of the average distance between EGFP+ nuclei, showed no increase in cell size in mutants compared to control embryos **(Figure S3)**. This suggests proliferation, rather than a change in cell size, as the mechanism underlying the enlarged CV diameter. Embryos lacking a clearly distinguishable CV were omitted from the analysis. Notably, the proportion of excluded embryos was higher in mutant embryos, when compared to CTRL or WT **(Table S1)**. This underscores pathophysiological effect also for N564D variant in which the percentage of discarded embryos reached 42,8%, compared to 0% for empty vector, 10% and 6,25% for the WT and WT + *pik3r1Mo* constructs, respectively. Despite the clonal expression, we only noted a tendency toward a compressed capillary bed in embryos with knocked-down expression, in contrast to the consistently pronounced phenotype observed in embryos overexpressing mutant *PIK3R1*. Although this tendency in knocked-down embryos did not reach statistical significance, it still led to observable alterations in the overall appearance of the caudal region. Overall, this indicates that the phenotype can be induced by mutant *PIK3R1*

alone, and that malformations are not due to a dosage effect. Indeed, overexpressing *PIK3R1*^{WT} did not result in malformations. Therefore, we hypothesize that the mosaic mutations act through a dominant mechanism on the pool of endogenous *PIK3R1*^{WT} by adversely affecting its regulatory activity on the p110-subunit. In short, mosaic overexpression of mutated *PIK3R1* is sufficient to induce a phenotype in embryos, despite the presence of endogenous *PIK3R1*. Furthermore, in the rescue experiment we did not observe an improvement, nor an exacerbation of the phenotype induced by the morpholino when attempting to rescue it with wt or mutated *PIK3R1*. This can be attributed to the fact that while the morpholino targeted the entire pool of endogenous *PIK3R1*, the plasmid induced only mosaic expression, which varied from embryo to embryo, and it was not integrated in all cells. Therefore, the relatively low mosaicism level of the injected constructs did not allow for a modulation of the generalized effect of the morpholino. However, we observed that mutant embryos with a higher rate of plasmid integration, and thus with a higher number of EGFP+ cells, showed a tendency towards a more severe malformation *(data not shown)*. These observations further support the hypothesis that *PIK3R1* pathogenic variants result in a dominant *PIK3R1* function.

We observed a strong specificity of the malformations for slow-flow vessels in zebrafish. Despite the presence of mutated *PIK3R1*-expressing cells (EGFP+) across different structures, including CV and CP, DA, intersegmental vessels (ISV) and dorsal longitudinal anastomotic vessels (DLAV), the abnormal phenotype was confined to the CV and CP. This suggests that fast-flow vessels, such as the DA, might be protected against the development of vascular abnormalities induced by *PIK3R1* mutations. This aligns with clinical observations, where CMDV malformations predominantly impact veins and capillaries, while arteries remain unaffected. However, further investigation is needed in order to gain a deeper understanding of this potential mechanism. In summary, we identified that capillary malformation associated with dilated veins (CMDV) is due to somatic *PIK3R1* or non-hotspot *PIK3CA* pathogenic

variants. Our findings suggest that somatic dominant *PIK3R1* and non-hotspot *PIK3CA* mutations could serve as a global mechanism for activation of class IA PI3K kinases, leading to CMDV. On the basis of primary cell isolations, we propose that the phenotype originates from mutant endothelial cells, which are an accessible target via the circulation. Currently, the management of CM typically involves laser ablation and surgery. However, our discovery on the mutated genes and dysregulated pathways underlying CMDV opens avenues for potential treatment of this condition using anti-cancer drugs targeting PI3K-signalling. Additionally, *in vivo* studies recapitulating the capillary-venous-specific phenotype observed in patients indicate zebrafish as a potential model for future drug screenings.

MATERIALS AND METHODS

Patient population and study approval

Written informed consent was obtained for all participants and approved by the ethical committee of the Medical Faculty at the University of Louvain, Brussels, Belgium (B403201629786) and the Centre Hospitalier Universitaire de Caen (France). All subjects, or their parent/guardian, included in this study consented to publication of the images in Figure 2.

Sample collection and DNA extraction

Our cohort consisted of 82 CM tissue samples. Tissue biopsies were collected during programmed surgeries and snap frozen in liquid nitrogen, or placed in RNAlater® solution (ThermoFisher Scientific). DNA from biopsies was extracted using the Wizard® Genomic DNA-purification kit (Promega), as previously described (Limaye et al., 2015).

Next-Generation-Sequencing (NGS) of tissular DNA and primary-EC and variant analysis

DNA samples were screened using IonTorrent technology, with two IonAmpliseq in-house designed panels (ThermoFisher Scientific), containing genes belonging to pathways involved in vascular anomalies. Libraries were prepared using the Ion AmpliSeq™ Library Kit 2.0, according to manufacturer's protocol (Pub. No. MAN006735, Life Technologies). Theoretical vertical coverage was set to a minimum of 1000X. Raw data were aligned against the human reference genome (hg19/GRCh37) using Ion Torrent Suite Server 5 (Life Technologies). Variants were called using the Torrent variant caller (version 5.8.0). Stringent filtering of the variants was performed with in-house developed software, Highlander (https://sites.uclouvain.be/highlander/). DNA was extracted from $CD31^+$ EC and $CD31^-$ cells using Wizard Genomic DNA Purification Kit (Promega). Cells were sequenced via targeted-NGS (1000x) and WES (median vertical coverage of 229x). Sanger sequencing was performed to confirm NGS sequencing results.

Cell culture, isolation of primary-EC and treatment with signaling-pathway inhibitors

Primary-EC from CMDV and CLVM patients were isolated from patient-tissues. Dissociated cells were grown on fibronectin-coated plates in ECGM-2 (Bio Connect) containing penicillin/streptomycin (Sigma). EC were isolated using antibodies against CD31 coupled to magnetic beads (Miltenyi). EC and HUVEC were cultured on fibronectin-coated (Millipore) plates in ECGM-2. CD31-negative cells were also kept and separately cultured in the same conditions. Cells were treated with 15nM rapamycin (LC Laboratories), 5µM BYL719 (LC Laboratories) for 48h, or with 1µM MK2206 (Bio Connect) for 24h. For starvation experiments, cells were grown in Endothelial Cell Basal Medium-2 without FCS and growth factors for 48h.

Immunofluorescence

Cells were grown on fibronectin-coated chamber slides (Sigma-Aldrich), fixed with acetone and stained with antibodies against CD31 and von Willebrand factor (vWF) (1:500, Dako). Rabbit-Alexa488 or mouse-Alexa594 were used as secondary antibodies (1:500, Thermo Fisher Scientific). Injected zebrafish embryos were selected to keep only those displaying fluorescent signal in vasculature and fixed in 4% PFA , stained for chicken anti-GFP (1:200, Aves labs), and subsequently, for FITC-conjugated goat anti-chicken (1:200, Aves labs). Images were captured on a fluorescent microscope (Leica) or on LSM710 (Zeiss) and processed with Fiji (version 2.9.0).

Western-blot analyses

Cell lysates from non-treated or drug-treated CMDV-EC, CLVM-EC and HUVEC were analyzed by western-blot. Quantification was performed using ImageJ. Statistical analyses were performed using GraphPad Prism 9.5.9. An unpaired two-tailed *t*-test with Welch's correction was used.

Site-specific mutagenesis of *PIK3R1*

Human *PIK3R1* (NM_181523.2) cDNA was synthesized from total RNA extracted from human tissue, cloned into pBlueScript II SK(+) vector. Mutagenesis was performed via PCR. The whole coding sequence was sequenced to verify the absence of undesired changes. *PIK3R1*^{WT} and mutant cDNAs were then transferred into the linearized UAS-p2A-H2B-EGFP expression vector.

Zebrafish strains

Handling of zebrafish was done according to FELASA guidelines (Aleström et al., 2020) Laboratory animals 54 (3), 213-224), in compliance with German and Brandenburg state laws, monitored by local authority for animal protection (LAVG, Brandenburg, Germany).

Plasmid and morpholino injection into zebrafish embryos

1nL of injection mix (plasmid and Tol2-transposase mRNA) was injected into embryos at one-cell stage. Empty vector (EV) UAS-H2B-EGFP was injected in the same manner, as negative control. 5ng of splicing-inhibiting morpholino pik3r1-MO, or std-Mo were injected for knockdown experiments. Knockdown efficiency was confirmed by RT-PCR from cDNA of injected embryos. For rescue experiments of endogenous pik3r1-knockdown, injection mix containing the expression vector and pik3r1-MO/std-MO in the same concentrations were injected into one-cell stage embryos. Confocal images were obtained using LSM 710 or LSM 880 Airyscan confocal laser microscopes (Zeiss) and ZEN 2 software (40x objective).

Quantification of caudal vein diameter, vascular bed breadth and extravascular space

The diameter of the embryonic zebrafish caudal vein was measured using Fiji. Three measurements were taken on each embryo (left, center and right side of the image). Comparisons were made using unpaired two-tailed t-test with Welch's correction (GraphPad Prism 9.5.9). Detection of the extravascular space was performed on maximum intensity Z-projection images using an in house-developed script based on EBImage (Pau et al., 2010), Reshape (Wickham, 2007) and Raster (Hijmans and van Etten, 2012) scripts, which allowed to circle and assign an ID to each empty space between vessels. This analysis was performed on n=5 embryos per condition and was only focused on the area in between DA (excluded) and CV (included).

Plasmid integration rate analysis

The rate of plasmid integration was determined by counting nuclei with EGFP (EGFP+) expression. We counted nuclei between DA (excluded) and CV (included). The counting was performed on confocal Z-stack images of the EGFP channel. Standard deviations are reported as measure of variability.

DATA AVAILABILITY STATEMENT

Data are available upon reasonable request. All data relevant to the study are included in the article or uploaded as supplementary information. The datasets supporting the current study have not been deposited in a public repository because data are not public due to privacy laws on patients. Some of the data may be requested by contacting to corresponding author.

ORCiDs

Martina De Bortoli, MSc, ORCID: 0009-0002-2455-1731

Angela Queisser, PhD, ORCID: 0000-0002-0993-9132

Van Cuong Pham, MSc, ORCID: 0000-0003-4787-7013

Anne Dompmartin, MD, PhD, ORCID: 0000-0003-0081-500X

Raphaël Helaers, PhD, ORCID: 0000-0002-7046-7867

Simon Boutry, MSc, ORCID: 0000-0002-3214-2981

Cathy Claus, MD, PhD, ORCID: 0009-0005-7560-7020

Frank Hammer, MD, ORCID: 0000-0003-0745-3830

An-Katrien De Roo, MD, ORCID: 0000-0002-0000-1260

Pascal Brouillard, PhD, ORCID: 0000-0001-9548-8229

Salim Abdelilah-Seyfried, PhD, ORCID 0000-0003-3183-3841

Laurence M. Boon, MD, PhD, ORCID: 0000-0001-8273-3328

Miikka Vikkula, MD, PhD, ORCID: 0000-0002-6236-338X

CONFLICT OF INTEREST

The authors state no conflict of interest.

ACKNOWLEDGEMENTS

Four of the authors of this publication are members of the Vascular Anomaly Working Group (VASCA WG) of the European Reference Network for Rare Multisystemic Vascular Diseases (VASCERN) - Project ID: 769036. We are grateful to all the family members for their invaluable participation. The authors thank Audrey Debue and Fabrice Cahay for expert technical assistance. These studies were financially supported by the Fonds de la Recherche Scientifique - FNRS Grants T.0240.23 & P.C005.22 (to MV), T.0146.16 and P.C013.20 (to LMB), and by the Fund Generet managed by the King Baudouin Foundation (Grant 2018-J1810250-211305), the Walloon Region through the FRFS-WELBIO strategic research programme (WELBIO-CR-2019C-06), and the European Union's Horizon 2020 research and innovation programme under grant agreement No 874708 (Theralymph)(all to MV). This project was also funded by the Swiss National Science Foundation under the Sinergia project nro CRSII5_193694 (LB/MV). The project has also received funding from the European Union's Horizon 2020 research and innovation programme under the Marie Skłodowska-Curie grant agreement No 814316 (project VACure) and Leducq foundation Networks of Excellence Program grant "ReVAMP" (LFCR Grant 21CVD03) (both to SS and MV).

P.B. is a Scientific Logistics Manager of the Genomics Platform of University of Louvain. The project was also supported by a Pierre M. fellowship. The authors thank the Genomics Platform of University of Louvain for IonTorrent PGM Next Generation Sequencing. We also thank the National Lottery, Belgium and the Foundation against Cancer (2010-101), Belgium for their

support to the Genomics Platform of University of Louvain and de Duve Institute, as well as the Fonds de la Recherche Scientifique - FNRS Equipment Grant U.N035.17 for the «Big data analysis cluster for NGS at UCLouvain».

AUTHOR CONTRIBUTIONS STATEMENT (CREDIT-COMPLIANT)

Conceptualization and design: MDB, PB, AQ, SS and MV. Data curation: MDB, CVP, SB, RH, PB, AQ and MV. Formal analysis: MDB, AQ, CVP. Patient data: AD, CC, FH, AKDR and LB. Software: RH. Supervision: SS and MV. Writing (original draft): MDB. Writing (review and editing): MDB, PB, SS, AKDR and MV. Resources: MV. Guarantor: MV.

All authors reviewed the results and approved the final version of the manuscript.

REFERENCES

Adams DM, Trenor CC, Hammill AM, Vinks AA, Patel MN, Chaudry G, et al. Efficacy and Safety of Sirolimus in the Treatment of Complicated Vascular Anomalies. Pediatrics 2016;137. https://doi.org/10.1542/PEDS.2015-3257.

Al-Olabi L, Polubothu S, Dowsett K, Andrews KA, Stadnik P, Joseph AP, et al. Mosaic RAS/MAPK variants cause sporadic vascular malformations which respond to targeted therapy. Journal of Clinical Investigation 2018;128:1496–508. https://doi.org/10.1172/JCI98589.

Aleström P, D'Angelo L, Midtlyng PJ, Schorderet DF, Schulte-Merker S, Sohm F, et al. Zebrafish: Housing and husbandry recommendations. Lab Anim 2020;54:213–24. https://doi.org/10.1177/0023677219869037.

Amyere M, Revencu N, Helaers R, Pairet E, Baselga E, Cordisco M, et al. Germline loss-of-function mutations in EPHB4 cause a second form of capillary malformation-arteriovenous malformation (CM-AVM2) deregulating RAS-MAPK signaling. Circulation 2017;136:1037–48. https://doi.org/10.1161/CIRCULATIONAHA.116.026886.

Asakawa K, Suster ML, Mizusawa K, Nagayoshi S, Kotani T, Urasaki A, et al. Genetic dissection of neural circuits by *Tol2* transposon-mediated Gal4 gene and enhancer trapping in zebrafish. Proceedings of the National Academy of Sciences 2008;105:1255–60. https://doi.org/10.1073/pnas.0704963105.

Bell LM, Holm A, Matysiak U, Driever W, Rößler J, Schanze D, et al. Functional assessment of two variants of unknown significance in TEK by endothelium-specific expression in zebrafish embryos. Hum Mol Genet 2021;31:10–7. https://doi.org/10.1093/hmg/ddab196.

Biesecker LG, Adam MP, Alkuraya FS, Amemiya AR, Bamshad MJ, Beck AE, et al. A dyadic approach to the delineation of diagnostic entities in clinical genomics. The American Journal of Human Genetics 2021;108:8–15. https://doi.org/10.1016/j.ajhg.2020.11.013.

Boon LM, Dekeuleneer V, Coulie J, Marot L, Bataille A-C, Hammer F, et al. Case report study of thalidomide therapy in 18 patients with severe arteriovenous malformations. Nature Cardiovascular Research 2022;1:562–7. https://doi.org/10.1038/s44161-022-00080-2.

Bornhorst D, Xia P, Nakajima H, Dingare C, Herzog W, Lecaudey V, et al. Biomechanical signaling within the developing zebrafish heart attunes endocardial growth to myocardial chamber dimensions. Nature Communications 2019 10:1 2019;10:1–10. https://doi.org/10.1038/s41467-019-12068-x.

Boscolo E, Limaye N, Huang L, Kang KT, Soblet J, Uebelhoer M, et al. Rapamycin improves TIE2-mutated venous malformation in murine model and human subjects. J Clin Invest 2015;125:3491–504. https://doi.org/10.1172/JCI76004.

Brouillard P, Schlögel MJ, Homayun Sepehr N, Helaers R, Queisser A, Fastré E, et al. Non-hotspot PIK3CA mutations are more frequent in CLOVES than in common or combined lymphatic malformations. Orphanet J Rare Dis 2021;16. https://doi.org/10.1186/S13023-021-01898-Y.

Chen L, Yang L, Yao L, Kuang XY, Zuo WJ, Li S, et al. Characterization of PIK3CA and PIK3R1 somatic mutations in Chinese breast cancer patients. Nature Communications 2018 9:1 2018;9:1–17. https://doi.org/10.1038/s41467-018-03867-9.

Cottrell CE, Bender NR, Zimmermann MT, Heusel JW, Corliss M, Evenson MJ, et al. Somatic PIK3R1 variation as a cause of vascular malformations and overgrowth. Genetics in Medicine 2021;23:1882–8. https://doi.org/10.1038/s41436-021-01211-z.

Couto JA, Huang L, Vivero MP, Kamitaki N, Maclellan RA, Mulliken JB, et al. Endothelial Cells from Capillary Malformations Are Enriched for Somatic GNAQ Mutations. Plast Reconstr Surg 2016;137:77e–82e. https://doi.org/10.1097/PRS.0000000000001868.

De Bortoli, M., Ivars, M., Revencu, N., Nassogne, M.-C., Lavarino, C., Paco, S., et al. Epilepsy with faint capillary malformation or reticulated telangiectasia associated with mosaic AKT3 pathogenic variants. American Journal of Medical Genetics Part A, 2016 e63551. https://doi.org/10.1002/ajmg.a.63551

Dogruluk T, Tsang YH, Espitia M, Chen F, Chen T, Chong Z, et al. Identification of Variant-Specific Functions of PIK3CA by Rapid Phenotyping of Rare Mutations. Cancer Res 2015;75:5341–54. https://doi.org/10.1158/0008-5472.CAN-15-1654.

Eerola I, Boon LM, Mulliken JB, Burrows PE, Dompmartin A, Watanabe S, et al. Capillary Malformation–Arteriovenous Malformation, a New Clinical and Genetic Disorder Caused by RASA1 Mutations. The American Journal of Human Genetics 2003;73:1240–9. https://doi.org/10.1086/379793.

Goss JA, Konczyk DJ, Smits P, Sudduth CL, Bischoff J, Liang MG, et al. Diffuse Capillary Malformation with Overgrowth Contains Somatic PIK3CA Variants. Clin Genet 2020;97:736. https://doi.org/10.1111/CGE.13702.

Gymnopoulos M, Elsliger MA, Vogt PK. Rare cancer-specific mutations in PIK3CA show gain of function. Proc Natl Acad Sci U S A 2007;104:5569–74. https://doi.org/10.1073/PNAS.0701005104.

Harbers VEM, Zwerink LGJM, Rongen GA, Klein WM, van der Vleuten CJM, van Rijnsoever IMP, et al. Clinical differences in sirolimus treatment with low target levels between children and adults with vascular malformations – A nationwide trial. Clin Transl Sci 2023;16:781–96. https://doi.org/10.1111/cts.13488.

Herwig L, Blum Y, Krudewig A, Ellertsdottir E, Lenard A, Belting H-G, et al. Distinct Cellular Mechanisms of Blood Vessel Fusion in the Zebrafish Embryo. Current Biology 2011;21:1942–8. https://doi.org/10.1016/j.cub.2011.10.016.

Jaiswal BS, Janakiraman V, Kljavin NM, Chaudhuri S, Stern HM, Wang W, et al. Somatic Mutations in p85α Promote Tumorigenesis through Class IA PI3K Activation. Cancer Cell 2009;16:463–74. https://doi.org/10.1016/j.ccr.2009.10.016.

Jin N, Keam B, Cho J, Lee MJ, Kim HR, Torosyan H, et al. Therapeutic implications of activating noncanonical PIK3CA mutations in head and neck squamous cell carcinoma. Journal of Clinical Investigation 2021;131. https://doi.org/10.1172/JCI150335.

Jordan M, Carmignac V, Sorlin A, Kuentz P, Albuisson J, Borradori L, et al. Reverse Phenotyping in Patients with Skin Capillary Malformations and Mosaic GNAQ or GNA11 Mutations Defines a Clinical Spectrum with Genotype-Phenotype Correlation. Journal of Investigative Dermatology 2020;140:1106-1110.e2. https://doi.org/10.1016/j.jid.2019.08.455.

Keppler-Noreuil KM, Parker VER, Darling TN, Martinez-Agosto JA. Somatic overgrowth disorders of the PI3K/AKT/mTOR pathway & therapeutic strategies. Am J Med Genet C Semin Med Genet 2016;172:402–21. https://doi.org/10.1002/AJMG.C.31531.

Kimmel CB, Ballard WW, Kimmel SR, Ullmann B, Schilling TF. Stages of embryonic development of the zebrafish. Dev Dyn 1995;203:253–310. https://doi.org/10.1002/AJA.1002030302.

Li X, Lau AYT, Ng ASN, Aldehaiman A, Zhou Y, Ng PKS, et al. Cancer-associated mutations in the p85α N-terminal SH2 domain activate a spectrum of receptor tyrosine kinases. Proc Natl Acad Sci U S A 2021;118. https://doi.org/10.1073/PNAS.2101751118/-/DCSUPPLEMENTAL.

Limaye N, Kangas J, Mendola A, Godfraind C, Schlögel MJ, Helaers R, et al. Somatic Activating PIK3CA Mutations Cause Venous Malformation. Am J Hum Genet 2015;97:914–21. https://doi.org/10.1016/j.ajhg.2015.11.011.

Nicoli S, Knyphausen CP, Zhu LJ, Lakshmanan A, Lawson ND. MiR-221 Is Required for Endothelial Tip Cell Behaviors during Vascular Development. Dev Cell 2012;22:418–29. https://doi.org/10.1016/j.devcel.2012.01.008.

Nakashima M, Miyajima M, Sugano H, Iimura Y, Kato M, Tsurusaki Y, et al. The somatic GNAQ mutation c.548G>A (p.R183Q) is consistently found in Sturge-Weber syndrome. J Hum Genet 2014;59:691–3. https://doi.org/10.1038/jhg.2014.95.

Ng PK-S, Li J, Jeong KJ, Shao S, Chen H, Tsang YH, et al. Systematic Functional Annotation of Somatic Mutations in Cancer. Cancer Cell 2018;33:450-462.e10. https://doi.org/10.1016/j.ccell.2018.01.021.

Pau G, Fuchs F, Sklyar O, Boutros M, Huber W. EBImage—an R package for image processing with applications to cellular phenotypes. Bioinformatics 2010;26:979–81. https://doi.org/10.1093/bioinformatics/btq046.

Petrova T V., Koh GY. Organ-specific lymphatic vasculature: From development to pathophysiology. Journal of Experimental Medicine 2018;215:35–49. https://doi.org/10.1084/jem.20171868.

Queisser A, Seront E, Boon LM, Vikkula M. Genetic Basis and Therapies for Vascular Anomalies. Circ Res 2021;129:155–73. https://doi.org/10.1161/CIRCRESAHA.121.318145/FORMAT/EPUB.

Rödel CJ, Otten C, Donat S, Lourenço M, Fischer D, Kuropka B, et al. Blood Flow Suppresses Vascular Anomalies in a Zebrafish Model of Cerebral Cavernous Malformations. Circ Res 2019;125:e43–54. https://doi.org/10.1161/CIRCRESAHA.119.315076.

Seront E, Biard JM, Van Damme A, Revencu N, Lengelé B, Schmitz S, et al. A case report of sirolimus use in early fetal management of lymphatic malformation. Nature Cardiovascular Research 2023;2:595–9. https://doi.org/10.1038/s44161-023-00280-4.

Siegel DH, Cottrell CE, Streicher JL, Schilter KF, Basel DG, Baselga E, et al. Analyzing the Genetic Spectrum of Vascular Anomalies with Overgrowth via Cancer Genomics. J Invest Dermatol 2018;138:957–67. https://doi.org/10.1016/j.jid.2017.10.033.

Uebelhoer M, Boon LM, Vikkula M. Vascular Anomalies: From Genetics toward Models for Therapeutic Trials. Cold Spring Harb Perspect Med 2012;2:a009688–a009688. https://doi.org/10.1101/cshperspect.a009688.

Uihlein LC, Liang MG, Fishman SJ, Alomari AI, Mulliken JB. Capillary-venous malformation in the lower limb. Pediatr Dermatol, vol. 30, 2013, p. 541–8. https://doi.org/10.1111/pde.12186.

Urick ME, Rudd ML, Godwin AK, Sgroi D, Merino M, Bell DW. PIK3R1 (p85α) is somatically mutated at high frequency in primary endometrial cancer. Cancer Res 2011;71:4061–7. https://doi.org/10.1158/0008-5472.CAN-11-0549/649998/AM/PIK3R1-P85-ALPHA-P85-IS-SOMATICALLY-MUTATED-AT.

Walton RG, Jacobs AH, Cox AJ. Pigmented lesions in newborn infants. Br J Dermatol 1976;95:389–96. https://doi.org/10.1111/j.1365-2133.1976.tb00840.x.

Westerfield M, Doerry E, Kirkpatrick AE, Driever W, Douglas SA. An on-line database for zebrafish development and genetics research. Semin Cell Dev Biol 1997;8:477–88. https://doi.org/10.1006/scdb.1997.0173.

Wickham H. Reshaping Data with the **reshape** Package. J Stat Softw 2007;21. https://doi.org/10.18637/jss.v021.i12.

TABLES

Individual	Gene symbol	NT change	AA change	VAF	Consensus prediction	Protein domain	DNA source	COSMIC ID
Tissue 1	***PIK3CA***	c.1133G>A	Cys378Tyr	7%	16	PI3K_C2	RNAlater	COSV55952006 (4x)
Tissue 2	***PIK3CA***	c.1357G>A	Glu453Lys	6%	16	PI3K_C2	RNAlater	COSV55874585 (82x)
Tissue 3	***PIK3CA***	c.1357G>A	Glu453Lys	3%	16	PI3K_C2	RNAlater	COSV55874585 (82x)
Tissue 4	***PIK3CA***	c.3129G>T	Met1043Ile	5%	11	PI3K_catalytic	RNAlater	COSV55878974 (85x)
Tissue 5	***PIK3R1***	c.1126G>A	Gly376Arg	8%	18	nSH2	Frozen Tissue	COSV57123316 (31x)
Tissue 6	***PIK3R1***	c.1690A>G	Asn564Asp	3%	13	PI3K_p85_iSH2	Frozen Tissue	COSV57124003 (49x)
Tissue 7*	***PIK3R1***	c.1690A>G	Asn564Asp	11%	13	PI3K_p85_iSH2	Frozen Tissue	COSV57124003 (49x)
Tissue 8	***PIK3R1***	c.1709T>C	Leu570Pro	4%	16	PI3K_p85_iSH2	RNAlater	COSV57123228 (3x)
Tissue 9**	***PIK3R1***	c.1718T>C	Leu573Pro	18%	16	PI3K_p85_iSH2	Frozen Tissue	COSV57124674 (11x)
EC-N564D*	***PIK3R1***	c.1690A>G	Asn564Asp	50%	13	PI3K_p85_iSH2	Primary EC	COSV57124003 (49x)
EC-L573P**	***PIK3R1***	c.1718T>C	Leu573Pro	50%	16	PI3K_p85_iSH2	Primary EC	COSV57124674 (11x)

Table 1: Characteristics of *PIK3CA* and *PIK3R1* identified variants.

VAF = Variant Allele Frequency; consensus prediction is defined as the number of algorithms predicting the variant to be damaging; the * and ** symbols indicate samples from the same individual, respectively.

Individual	Age at operation	Sex	Gene	Nucleotide change	Hypotrophy limb	Hypertrophy limb	Pain (VAS scale/10)	D-Dimers
Tissue 1	55	F	***PIK3CA***	c.1357G>A	Left leg (12mm length)	Mild (girth)	5 (episodes of 8)	Normal
Tissue 2	17	M	***PIK3CA***	c.1357G>A	Hypoplasia	-	7 in infancy	Normal (up to 605ng/mL when in pain)
Tissue 3	43	F	***PIK3CA***	c.3129G>T	-	-	3	Normal
Tissue 4	41	F	***PIK3CA***	c.1133G>A	-	Mild left leg (length 9mm; thigh girth 6cm)	6 (episodes of 9)	Normal
Tissue 5	14	F	***PIK3R1***	c.1126G>A	-	Mild (girth)	3-4	Normal
Tissue 6	39	F	***PIK3R1***	c.1690A>G	-	-	5	Normal
Tissue 7	26	F	***PIK3R1***	c.1690A>G	-	-	4-5	N/A
Tissue 8	10	M	***PIK3R1***	c.1709T>C	-	-	5 in infancy	Normal
Tissue 9	24	F	***PIK3R1***	c.1718T>C	Left leg (13mm length)	-	4-5	Normal

Table 2: Clinical characteristic of patients with *PIK3R1* and *PIK3CA* variants.

FIGURE LEGENDS

Figure 1: PIK3CA and PIK3R1 protein structures and distribution of identified variants. **(a)** *PIK3R1* protein (p85) and its functional domains. Variants localized in the nSH2 domain (n=1) and in the PI3K_P85_iSH2 domain (n=3). L570P and L573P variants are predicted to be pathogenic, but lack experimental validation. **(b)** *PIK3CA* (p110) and its functional domains. Variants reported in black, localized in the Ca^{2+} binding domain (n=2), and in PI3K catalytic domain (n=1). Hotspot *PIK3CA* mutations, in grey. Cancer hotspot regions are highlighted in light blue.

Figure 2: Clinical phenotype of CMDV patients with PIK3R1 or non-hot post PIK3CA variants. Patients characterized by localized capillary malformations (CM) and dilated veins visible on skin and MRI (white arrows). **(a)** Patients with smaller lesions and less prominent veins. **(b)** Patients with more extensive lesions and strongly prominent veins. **(c)** Progression of lesion in individual 2 from 7 to 21yo: veins became more prominent, dilated and CM turned from reddish to purplish color. **(d)** MRI (fat suppression sequence, 1.5T) of the lower limbs of patients 4, 5 and 7 showing hyperintense slow-flowing blood in dilated veins of the subcutaneous tissues. All subjects, or their parent/guardian, included in this study consented to publication of the images shown in this figure.

Figure 3: Endothelial cells (EC) isolated from CMDV patients. (a) $CD31^+$ selected-EC and $CD31^-$ cells. $CD31^+$ EC show the typical cobblestone morphology; $CD31^-$ cells look more elongated. **(b)** Immunofluorescence of $CD31^+$ selected-EC expressing von Willebrand factor (vWF) and CD31. Scale bar = 1000µM.

Figure 4: Western-blot analysis of AKT and ERK-phosphorylation and treatment with PI3K pathways inhibitors (a) Patient-derived EC-N564D display AKT-phosphorylation. pAKT is decreased after treatment with rapamycin and BYL719 (48 hours) or MK2206 (24h). **(b)** Patient-derived EC-L573P display AKT-phosphorylation. pAKT is decreased after treatment with rapamycin and BYL719 (48 hours) or MK2206 (24h). **(c)** Patient-derived EC-N564D show ERK-phosphorylation. pERK is decreased upon treatment with BYL719, but not with rapamycin or MK2206 **(d)** Patient-derived EC-L573P show ERK-phosphorylation. pERK is decreased upon treatment with BYL719 and MK-2296, but not with rapamycin. α-actinin as loading control. PIK3CA-hs (hotspot) EC, are primary-cells from a CLVM patient (H1047R PIK3CA mutation). Error bars are shown as measure of variability and represent the standard deviation (STD). Experiments were repeated N=5 times for EC-N564D cells. Due to a shortage of surgical resected tissue and limited number of viable EC-L573P passages, AKT/pAKT and ERK/pERK were repeated N=2 and N=1 times, respectively.

Figure 5: Endothelial-specific overexpression of mutated *PIK3R1* in *Tg(fli1a:Gal4FF^{ub53};UAS:RFP)*-positive zebrafish embryos. Normal and inverted images. EGFP+ cells (magenta) contain the injected plasmid. Caudal Vein (CV, red), Dorsal Aorta (DA, yellow), Capillary Plexus (CP, blue). **(a)** Embryos with normal development of trunk vasculature. **(b-c)** Embryos injected with pUAS-p2A-H2b-EGFP (EV) and pUAS-*PIK3R1^{WT}*-p2A-H2b-EGFP: normal development of trunk vasculature. **(d-f)** Embryos injected with pUAS-*PIK3R1*-p2A-H2b-EGFP expressing mutated-*PIK3R1:* CV enlargement and CP disruption. **(g)** Quantification of area between CV and DA occupied by the capillary bed: ratio between intravessel and intervessel space. **(h)** Quantification of CV diameter. **(i)** Quantification of plasmid-integration rate in zebrafish endothelium: EGFP+-cells found in capillary-venous plexus. Plotted are averages normalized on the number of embryos for each condition. Each

blue dot corresponds to one embryo. Scale bar = 50µM. Error bars are shown as measure of variability and represent the standard deviation (STD). Number of biological replicates: uninjected (N=19), EV (N=10), PIK3R1^{WT} (N=9), PIK3R1^{N564D} (N=4), PIK3R1^{L570P} (N=8), PIK3R1^{L573P} (N=9). Embryos in which the CV was not readily distinguishable were discarded.

Figure 6: PI3K-AKT-mTOR signaling and RAS-RAF-MEK-ERK signaling in vascular anomalies. In red inhibitors of the signalling pathway: PIK3CA-inhibitor Alpelisib (BYL719), AKT-inhibitor MK-2209 and mTOR-inhibitor rapamycin (Sirolimus).

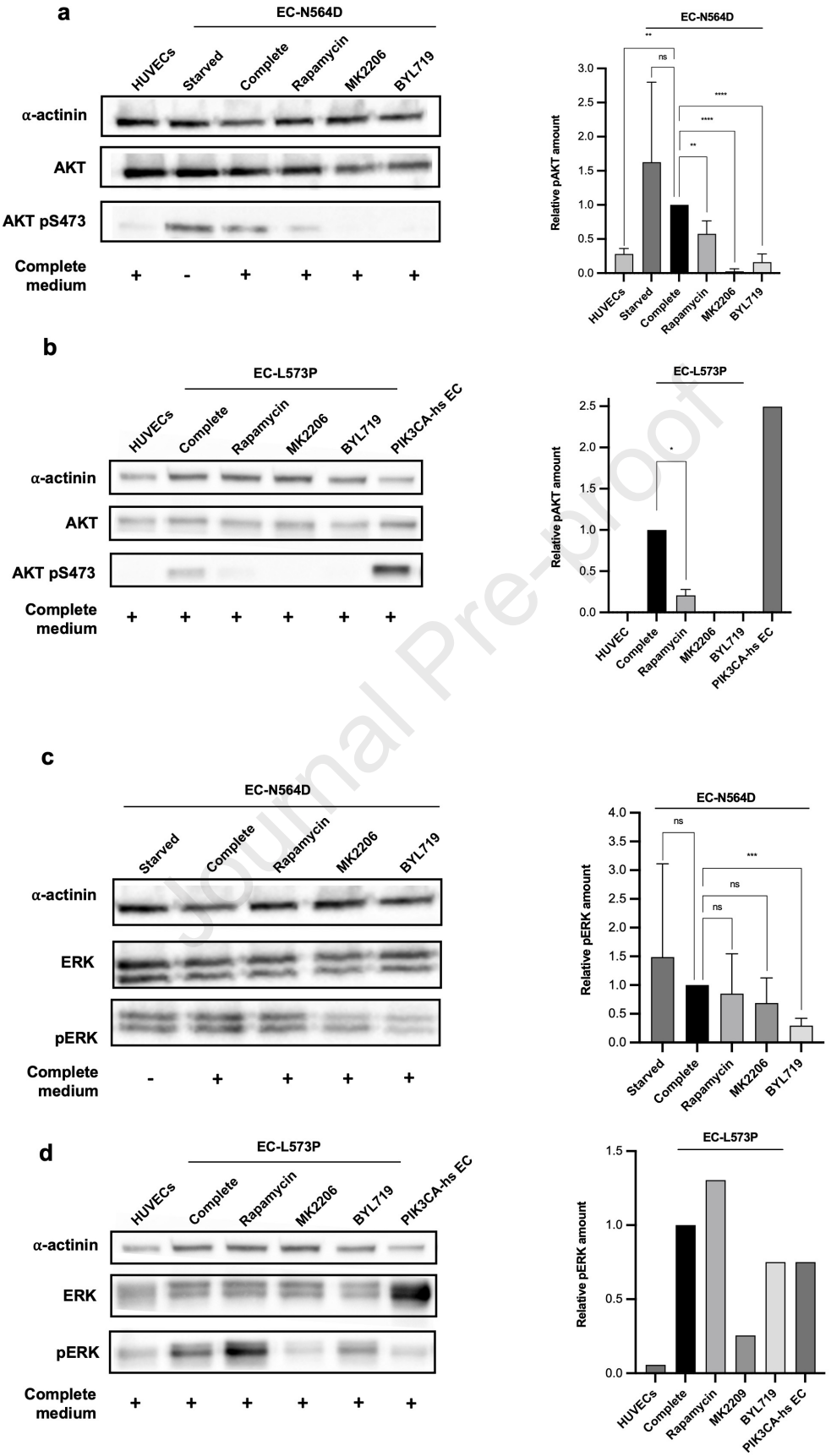
a
EC-N564D
HUVECs
Starved
Complete
Rapamycin
MK2206
BYL719
α-actinin
AKT
AKT pS473
Complete medium
+ - + + + +
EC-N564D
Relative pAKT amount
HUVECs
Starved
Complete
Rapamycin
MK2206
BYL719
b
EC-L573P
HUVECs
Complete
Rapamycin
MK2206
BYL719
PIK3CA-hs EC
α-actinin
AKT
AKT pS473
Complete medium
+ + + + + +
EC-L573P
Relative pAKT amount
HUVEC
Complete
Rapamycin
MK2206
BYL719
PIK3CA-hs EC
c
EC-N564D
Starved
Complete
Rapamycin
MK2206
BYL719
α-actinin
ERK
pERK
Complete medium
- + + + +
EC-N564D
Relative pERK amount
Starved
Complete
Rapamycin
MK2206
BYL719
d
EC-L573P
HUVECs
Complete
Rapamycin
MK2206
BYL719
PIK3CA-hs EC
α-actinin
ERK
pERK
Complete medium
+ + + + + +
EC-L573P
Relative pERK amount
HUVECs
Complete
Rapamycin
MK2209
BYL719
PIK3CA-hs EC

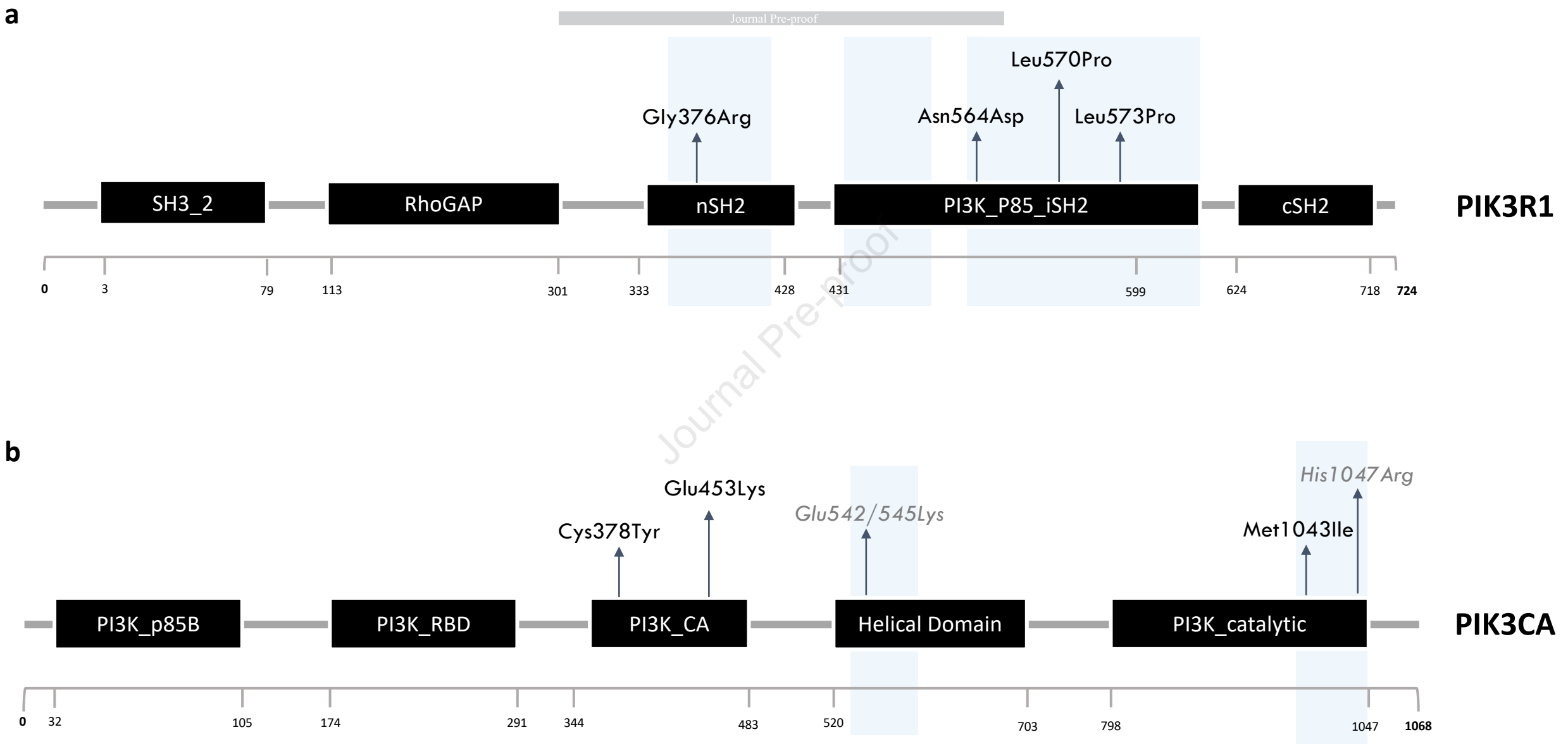

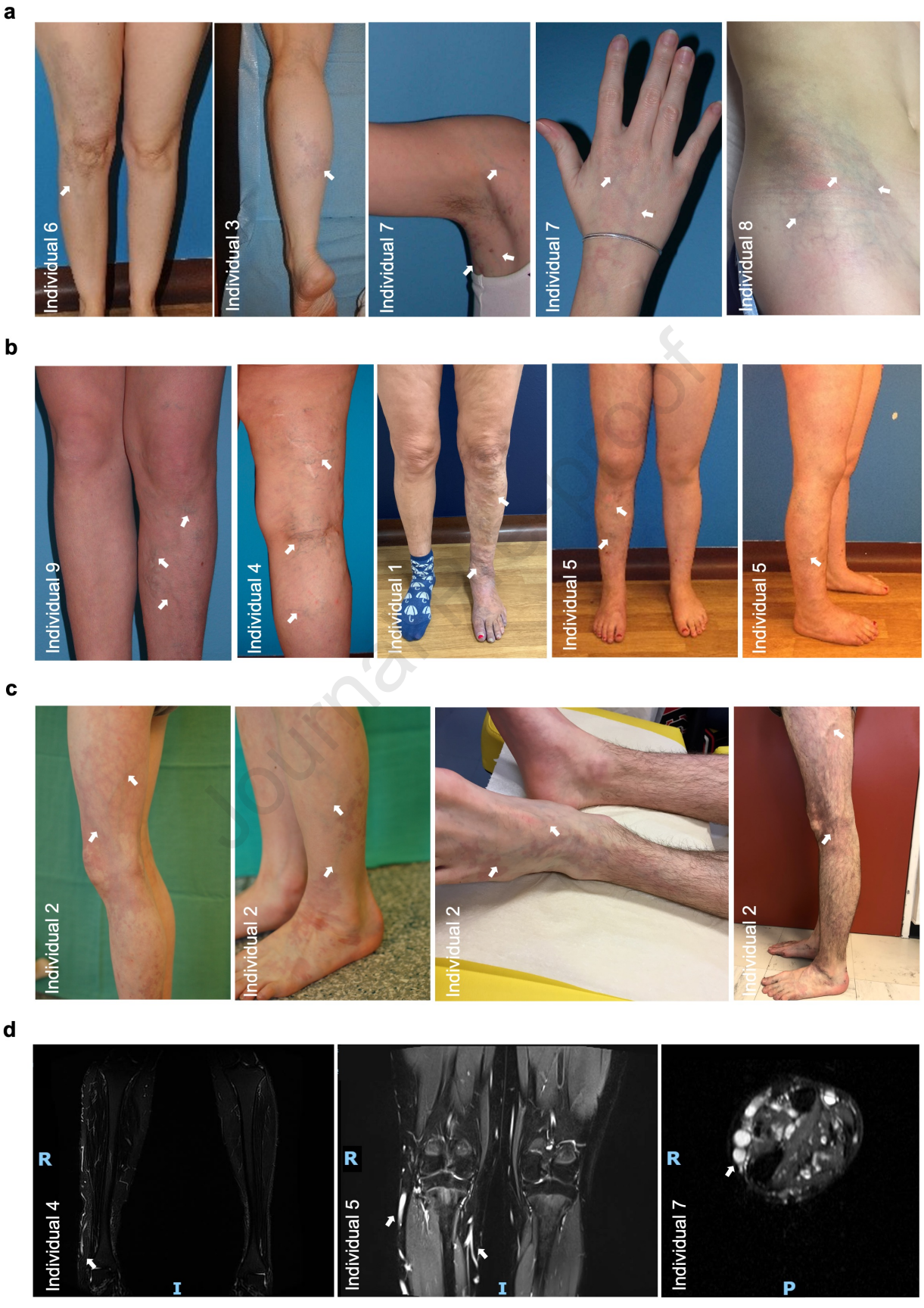

a

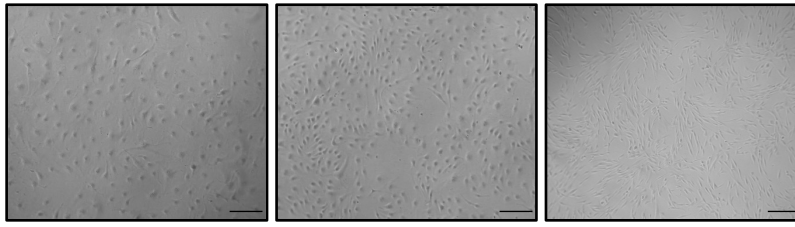

CD31⁺ EC-N564D | CD31⁺ EC-L573P | CD31⁻ cells

b

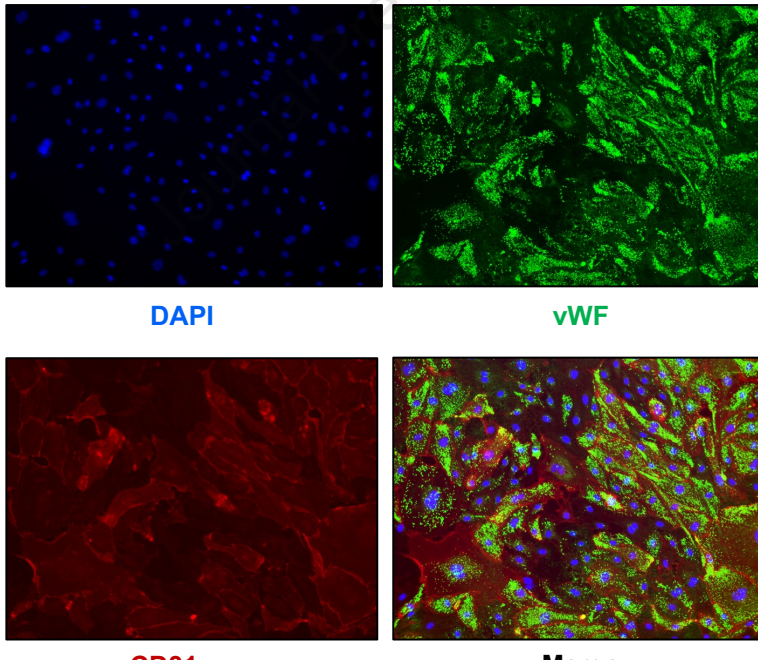

DAPI | vWF

CD31 | Merge

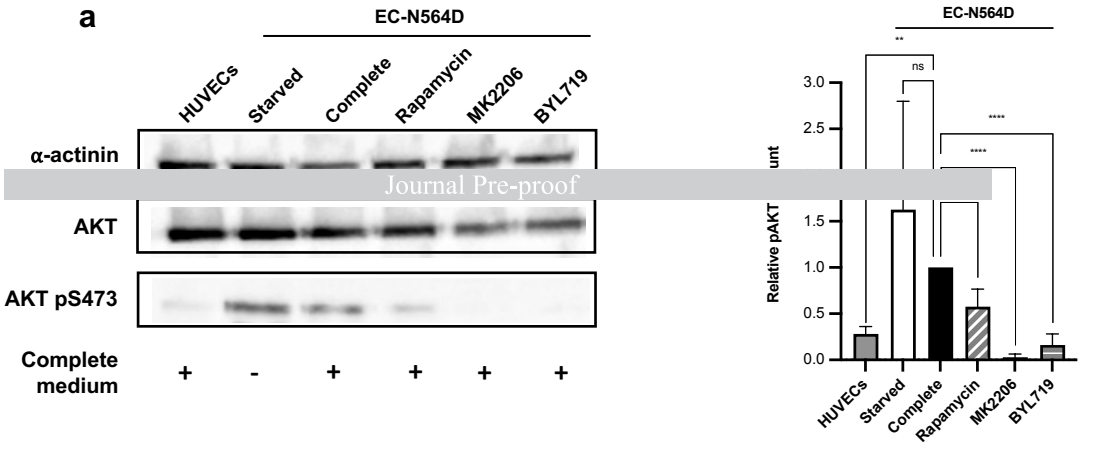

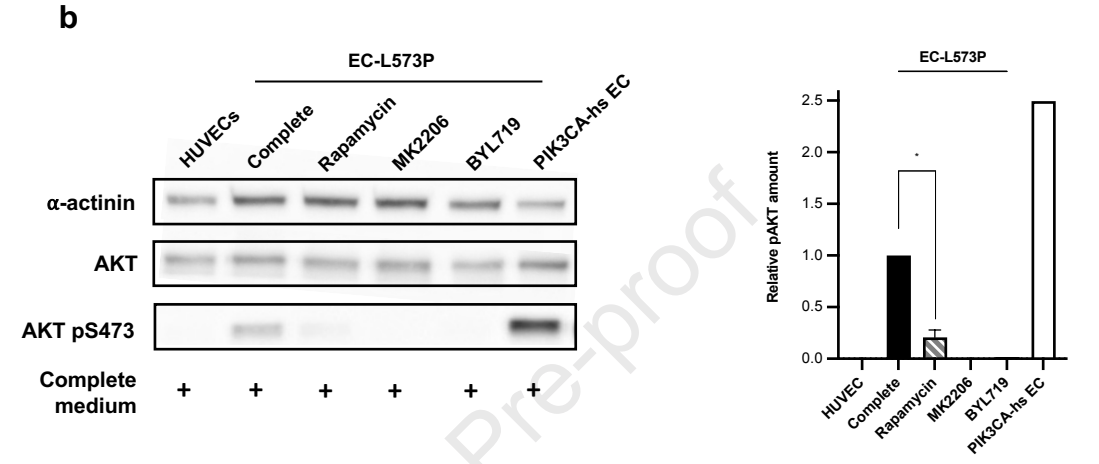

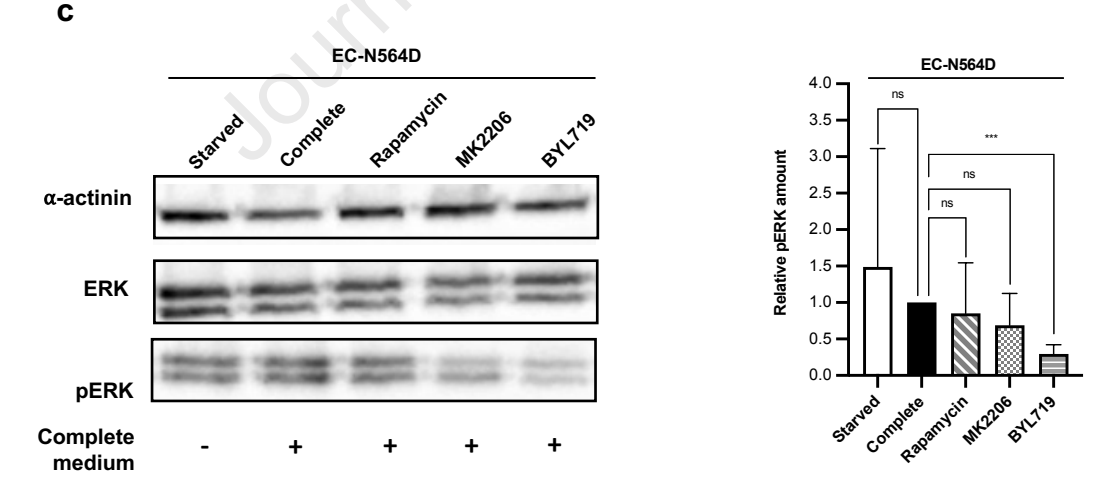

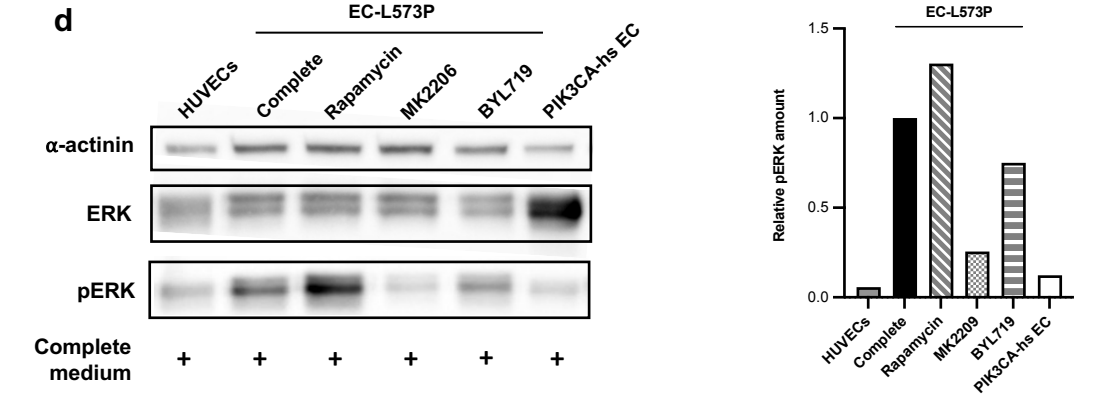

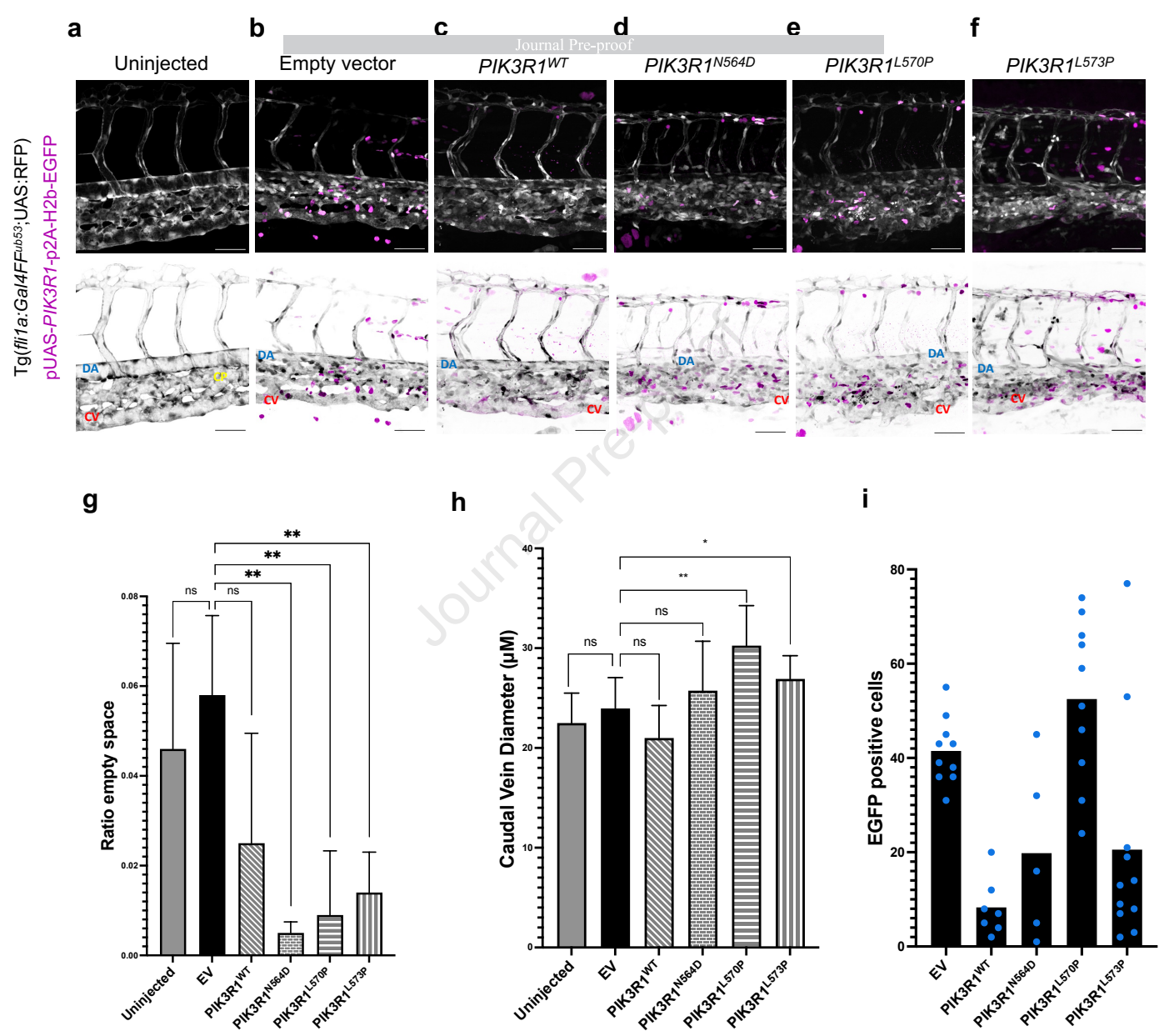

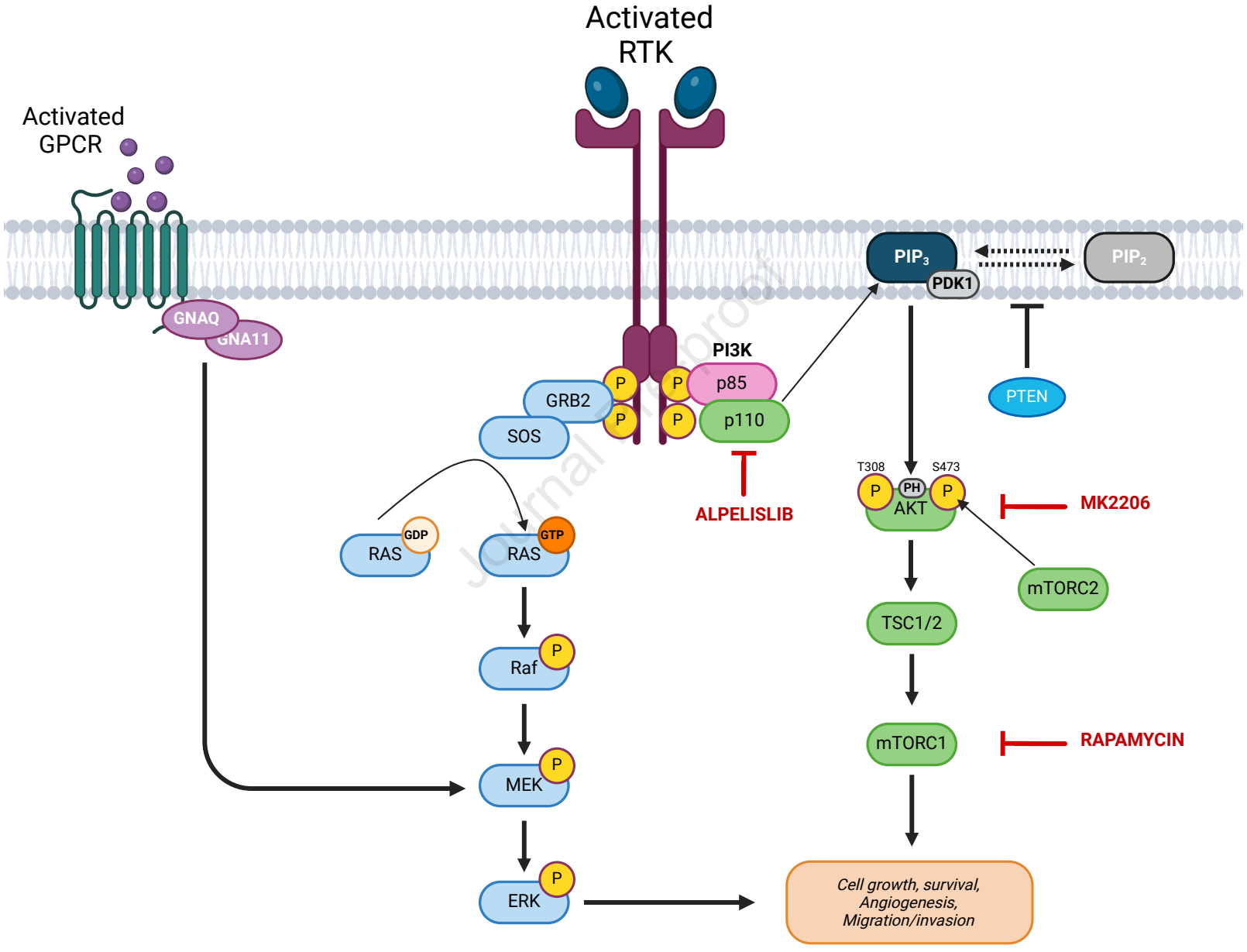

	Condition	Total n. of embryos	N. analyzed embryos	N. of discarded embryos	% of discarded embryos
	Uninjected	19	19	0	0%
	pik3r1Mo	33	29	4	12%
	EV	10	10	0	0%
	PIK3R1^{WT}	10	9	1	10%
	PIK3R1^{N564D}	7	4	3	42,8%
	PIK3R1^{L570P}	10	8	2	20%
	PIK3R1^{L573P}	13	9	4	30,7%
+ pik3r1Mo	**EV**	10	10	0	0%
	PIK3R1^{WT}	16	15	1	6,2%
	PIK3R1^{N564D}	21	14	7	33,3%
	PIK3R1^{L570P}	18	14	4	22,2%
	PIK3R1^{L573P}	11	9	2	18,1%

Table S1: numbers of embryos considered for the CV diameter analysis. Embryos that did not display a clearly distinguishable CV were excluded from the analysis.

SUPPLEMENTARY MATERIALS AND METHODS

Sample collection and DNA extraction

Samples of patients with a capillary malformation were collected at Saint Luc University Hospitals in Brussels (Belgium) and at the Centre Hospitalier Universitaire de Caen (France). Our cohort consisted of a total of 82 CM tissue samples. Tissue biopsies were collected during programmed surgeries and snap frozen in liquid nitrogen or placed in RNAlater® solution (Thermo Fisher Scientific). DNA from biopsies was extracted using the Wizard® Genomic DNA purification-kit (Promega), as previously described (Limaye et al., 2015). DNA was subsequently quantified using NanoDrop 8000 (Thermo Fisher Scientific) and Qubit 2.0 (Thermo Fisher Scientific).

Targeted Next-Generation Sequencing (NGS) of tissular DNA and variant analysis

DNA samples were screened using IonTorrent technology, with two IonAmpliseq in-house designed panels (Thermo Fisher Scientific). Both panels contained genes belonging to pathways involved in vascular anomalies, such as PI3 Kinase and MAP Kinase signaling. Libraries were prepared using the Ion AmpliSeq™ Library Kit 2.0, according to the manufacturer's protocol (Pub. No. MAN006735, Life Technologies). For high-quality DNA extracted from fresh frozen tissues, 25ng of DNA were employed for each of the two primer pools (2X). The kit generated libraries composed of amplicons of around 180-200pb. For low-quality DNA, extracted from RNAlater samples, 10ng of DNA for each of the two primer pools (5X) were employed. The kit generated libraries composed of amplicons of around 100-110pb. DNA sequencing was performed on an Ion Proton sequencer (Thermo Fisher Scientific). Theoretical vertical coverage was set to a minimum of 1000X. Raw data were aligned against the human reference genome (hg19/GRCh37) using the Ion Torrent Suite Server 5 (Life Technologies) to generate *.bam* (binary alignment map) -files. Variants were called using the Torrent variant caller (version 5.8.0). Filtering of the variants was performed with our in-house developed software, Highlander (https://sites.uclouvain.be/highlander/). Applied filters allowed to obtain variants fulfilling all the following criteria: (a) passed quality control, (b) missense, non-sense and consensus splice site-changes, (c) <0,005% allele frequency in the gnomAD database including WES data from 125.748 unrelated individuals (https://gnomad.broadinstitute.org/), (d) not detected in more than 100 samples from individuals with unrelated pathologies in the in-house database of 1737 somatic samples, (e) >1% of alternative allele on the total coverage, (f) >5 alternative reads on the total of depth reads, (f) for missense variants, predicted to affect protein function by at least 5 out of 20 algorithms available in Highlander (Mutation Taster, FATHMM, FATHMM-XF, Polyphen2, Provean, SIFT4G, Mutation Assessor, MCAP, LRT, Lists2, Deogen, ClinPred, BayesDel, PrimateAl, MetaSVM, CADD phred, VEST, REVEL, MVP, MutPred). Variants present in the COSMIC (Catalogue Of Somatic Mutations In Cancer) (https://cancer.sanger.ac.uk/cosmic) database were considered as particularly relevant.

Cell culture, isolation of primary-endothelial cells and treatment with signaling pathway inhibitors

Primary ECs from CMDV and CLVM patients were isolated from tissues by cutting them into small pieces (1-3 cm^2) and digesting with a mixture of 0.04% dispase II (Gibco), 0.25% collagenase A (Sigma-Aldrich) and 0.01% DNAse I (Sigma-Aldrich). Dissociated cells were grown on fibronectin-coated (Millipore) plates in ECGM-2 containing penicillin/streptomycin (Sigma) until confluency. ECs were isolated using an antibody against CD31 coupled to magnetic beads (Miltenyi) and the obtained $CD31^+$ cells were cultured on fibronectin-coated plates in ECGM-2. $CD31^-$ cells were also kept and separately cultured in the same conditions. Cobblestone cell morphology of the $CD31^+$ cells was determined using a bright field

microscope (Zeiss). For drug testing, ECs were grown in complete medium and treated with 15nM rapamycin (LC Laboratories) or 5µM BYL719 (LC Laboratories) for 48 hours, or with 1µM MK2206 (Bio Connect) for 24 hours. For starvation experiments, ECs were grown in Endothelial Cell Basal Medium-2 without FCS and growth factors for 48 hours. Human umbilical vein endothelial cells (HUVEC) were grown on fibronectin coated plates in complete ECGM-2 (*Endothelial Cell Growth Medium 2*) (Bio-Connect). Experiments were only performed twice for EC-L573P, due to shortage of surgical resected tissue and limited number of passages after which EC continue to grow.

Cell immunofluorescence

Cells were grown on fibronectin-coated chamber slides (Sigma-Aldrich), fixed with acetone and stained with antibodies against CD31 and von Willebrand factor (vWF) (1:500, Dako). Rabbit-Alexa488 or mouse-Alexa594 were used as secondary antibodies, respectively (1:500, Thermo Fisher Scientific). Images were captured on a fluorescent microscope (Leica).

Sequencing of DNA extracted from primary cells

DNA was extracted from $CD31^+$ ECs as well as from $CD31^-$ cells using the Wizard Genomic DNA Purification Kit (Promega). Besides Targeted NGS, DNA underwent whole exome sequencing (WES) using the Twist capture-kit and Illumina sequencing on a Novaseq machine (performed by Macrogen), achieving a median vertical coverage of 229x. Sequences were aligned to the reference human genome (hg38) and processed with Highlander, as described above. Sanger sequencing was performed to confirm the *PIK3R1* NGS sequencing results through Eurofins Genomics, with primers: forward *5'-GACAGGAAGAGAAGCCACGC-3'* and reverse *5'-GCCCAACCACTCGTTCAACTTC-3'*. Chromatograms were analyzed using CLC Main Workbench (QIAGEN).

Western-blot analyses

Cell lysates from non-treated or drug-treated CMDV-EC, CLVM-EC, HUVEC and $HUVEC^{PIK3CA\text{-}E545K}$ were analyzed by western-blot using antibodies against α-actinin (1:1000, #6487 Cell Signaling), AKT (1:1000, #9272 Cell Signaling), pAKT Ser473 (1:1000, #9271 Cell Signaling), p44/42 MAPK (Erk1/2) (1:1000, #9102 Cell Signaling), and phospho-p44/42 MAPK (Erk1/2) Thr202/Tyr204 (#9101, Cell Signaling). Quantification was performed using ImageJ. Statistical analysis of western-blot quantification data was performed using GraphPad Prism (version 9.5.9). An unpaired two-tailed *t*-test with Welch's correction was used.

Zebrafish strains

Handling of zebrafish was done according to FELASA guidelines (Westerfield et al., 1997), in compliance with German and Brandenburg state laws, carefully monitored by the local authority for animal protection (LAVG, Brandenburg, Germany). The following stable lines of zebrafish were maintained under standard conditions as previously described *(Westerfield et al., 2000)*: *Tg(kdrl:EGFP)^{s843}* (Jin et al., 2005)*; Tg(fli1a:Gal4FF)^{ubs3}* (Herwig et al., 2011)*; Tg(UAS:RFP)^{nkuasrfp1a}* (Asakawa et al., 2008)*; Tg(UAS:lifeactRFP)^{mu262}* (Rödel et al., 2019).

Site-specific mutagenesis of *PIK3R1*

Human *PIK3R1* (NM_181523.2) cDNA was synthesized from total RNA extracted from human tissue, using RevertAid H Minus First Strand cDNA Synthesis kit (ThermoFisher Scientific, #K1632), cloned into the pBlueScript II SK vector by EcoRI restriction enzyme cloning. Mutagenesis primers were designed using the QuikChange II XL Primer Design-tool (Agilent). *In vitro* site-directed mutagenesis was performed via PCR using Pfu Turbo polymerase (ThermoFisher Scientific, #EP0501) followed by *DpnI* enzyme digestion. The whole coding

sequence of the gene was sequenced to confirm the presence of the nucleotide change of interest and exclude undesired changes. *PIK3R1* wild-type and mutant cDNAs were transferred into the linearized UAS-p2A-H2B-EGFP expression vector using the In-Fusion Snap Assembly Master Mix (Takara Bio, #638954), following manufacturer's protocol (Primers: *5'-CACACGAATTCCTGCAGCCCATGAGTGCTGAGGGGTACCAGTA-3'* forward, *5'-AAATTAGTAGCACCAGAACC-TCGCCTCTGCTGTGCATATACTG-3'* reverse). Plasmids were purified with the PureYield Plasmid Midiprep System (Promega, #A2492) and sequence-verified.

Plasmid and morpholino injection into zebrafish embryos

Plasmids were prepared in an injection mix containing 20ng/µL of plasmid and 20ng/µL of Tol2-transposase mRNA (co-injected to facilitate genomic integration of the plasmid. The plasmid was based on a UAS promoter, followed by the gene of interest. 1nL of injection mix (plasmid and Tol2-transposase mRNA) was injected into transgenic Tg(fli1a:Gal4FF)$^{ubs3/+}$ embryos at one cell stage, in order to overexpress *PIK3R1* variants specifically in endothelial cells with the GAL4-UAS system. Additionally, we used the combination of transgenic lines Tg(fli1a:Gal4FF)$^{ubs3/+}$;Tg(UAS:RFP)$^{nkuasrfp1a/+}$ to confirm the Gal4 presence, based on the expression of RFP fluorescent proteins. Empty vector (EV) of UAS-H2B-EGFP was injected in the same manner, as a negative control. For endogenous pik3r1 knockdown experiments, either 5ng of splicing inhibiting-morpholino pik3r1-MO (5'-GTATGGTATATTTACCTGGAGCTGC-3'; GeneTools, LLC, USA) (1ng of 0.59mM, refer to (Nicoli et al., 2012) or equivalent amount of standard control morpholino std-MO (5'-CCTCTTACCTCAGTTACAATTTATA-3'; GeneTools, LLC, USA) was injected into one-cell staged embryos. Knockdown efficiency was confirmed by semi-quantitative RT-PCR from cDNA of injected embryos using the following primers: forward 5'-CCCAGCACTCTTCAGACATC-3'; reverse 5'-TTTAGTGGAGGCATCTCGGA-3'). Assessment of the disappearance of endogenous amplified fragment was performed on agarose gel. For rescue experiments of endogenous pik3r1 knockdown, injection mixes containing plasmid and pik3r1-MO or std-MO were prepared with same concentrations and injected into one-cell stage embryos.

Imaging at confocal microscope

Injected embryos were kept under standard condition at 28.5°C and treated with 1-Phenyl-2-thiourea (PTU, Sigma) from 24 hour-post-fertilization (hpf). Embryos were manually dechorionated in between 48 to 52hpf and selected under Leica fluorescent microscope for RFP-vascular and EGFP reporter expression. For confocal imaging, embryos were anaesthetized with 4mg/mL 3-aminobenzoic acid ethyl ester (Tricaine/MS-222) (Sigma) and laterally mounted in 35mm glass bottom dishes using 1% low-melting agarose (LMA) containing 0,17mg/mL tricaine. Confocal images were obtained using either LSM 710 or LSM 880 Airyscan confocal laser microscope (Zeiss) and ZEN 2 software, with 40x objective for imaging of the trunk and caudal vasculatures. Maximum intensity Z-projections of captured images were generated and analyzed using Fiji (version 2.9.0).

Quantification of caudal vein diameter and vascular bed breadth

The diameter of the embryonic zebrafish caudal vein (CV) was measured using Fiji. Three measurements were taken on each embryo (on the left, center and right side of the image). The degree angle between the head and the neck of the fish was used to determine the developmental stage (Kimmel et al., 1995). Embryos in which the CV was not easily discernible were omitted from the analysis. Comparisons were made using unpaired two-tailed t-test with Welch's correction (using GraphPad Prism 9). Standard deviations are reported as a measure of

variability. For knockdown experiments, comparisons were made between uninjected or standard control oligo injected-embryos and MO-injected embryos. For rescue and overexpression experiments, comparisons were done between embryos injected with EV together with morpholino or EV only and those injected with *PIK3R1*-expression vectors.
To investigate whether the enlarged CV phenotype in mutant fish resulted from an enlargement of cells constituting the CV or rather from an increase in the number of cells, we measured the distance between neighboring EGFP+ nuclei (for plasmid-injected fish) or between one nucleus and its neighboring ones (for Mo-injected fish), as previously described by (Bornhorst et al., 2019). Measurements were done using the Imaris software.

Zebrafish immunofluorescence

Injected zebrafish embryos were selected to keep only those displaying fluorescent signal in the vasculature and then anaesthetized with Tricaine (Sigma) at 56 hpf and fixed in 4% PFA overnight at 4°C. Subsequently, they were washed in PBST (Phosphate Buffered Saline with 3% Tween) before blocking with 5% of NGS (Normal Goat Serum) in PBST for 2 hours, followed by incubation overnight in chicken anti-GFP (1:200, Aves labs). Embryos were then washed in PBST and incubated overnight with FITC-conjugated goat anti-chicken (1:200, Aves labs). Primary and secondary antibodies were diluted in PBST containing 0.2% Triton X-100, 1% BSA and 5% NGS. Stained embryos were mounted in SlowFade Gold (Thermo Fisher Scientific) and imaged on LSM 710 (Zeiss). Images were processed with Fiji as mentioned above.

Quantification of extravascular space

Detection of the extravascular space was performed on maximum intensity Z-projection images using an *in house*-developed script based on EBImage (Pau et al., 2010), Reshape (Wickham, 2007) and Raster (Hijmans and van Etten, 2012) scripts, which allowed to circle and assign an ID to each empty space between vessels. The data obtained were manually cleaned from false-positives in order to keep only the values corresponding to empty spaces on the original confocal image. Each empty space was considered as an ellipse. The final value of the total empty area was then calculated as follows:

$$A = \pi ab$$

The value normalized on the total size of the image and the total area occupied by the vascular bed is represented as a ratio, and was performed as follows:

$$Area_{total} = image\ area$$
$$Area_{empty\ space} = sum\ of\ all\ areas\ calculated\ on\ clean\ data$$
$$Area_{to\ remove} = Area_{total} - Area_{empty\ space}$$
$$Area_{of\ interest} = Area_{total} - Area_{to\ remove}$$
$$Ratio = \frac{Area_{empty\ space}}{Area_{to\ remove}}$$

This analysis was performed on n=5 embryos per condition and was only focused on the area in between the dorsal aorta (DA, excluded) and the CV (included).

Plasmid integration rate analysis

The rate of plasmid integration was determined by counting nuclei with EGFP (EGFP+) expression. We counted nuclei between the DA (excluded) and the CV (included). The counting was performed on confocal Z-stack images of the EGFP channel. Standard deviations are reported as measure of variability.

SUPPLEMENTARY TABLES LEGEND

Table S1: numbers of embryos considered for the CV diameter analysis. Embryos that did not display a clearly distinguishable CV were excluded from the analysis.

SUPPLEMENTARY FIGURES LEGEND

Supplementary Figure 1: Knockdown and rescue of *PIK3R1* expression in Tg*(fli1a:Gal4FF^{ub53};UAS:RFP)*-positive zebrafish embryos. Normal and inverted images. EGFP+ cells (magenta) integrated injected plasmid. Caudal Vein (CV, red), Dorsal Aorta (DA, yellow), Capillary Plexus (CP, blue). **(a)** Embryos injected with spliced-*pik3r1Mo* and uninjected control. Increased CV diameter, but no CP disruption as effect of *PIK3R1*-knockdown. **(b)** Embryos injected with *pik3r1Mo* and pUAS-p2A-H2b-EGFP (EV) or pUAS-*PIK3R1*-p2A-H2b-EGFP (wt/mutated) fail to rescue phenotype given by *pik3r1Mo* knockdown. **(c-d)** Quantification of CV diameter and area in between CV and DA, occupied by capillary bed, show no difference when knockdown rescued, whether wt or mutant-*PIK3R1* expressed. **(e)** Quantification of plasmid-integration rate in zebrafish endothelium: number of EGFP+ cells found in capillary-venous plexus. Plotted averages normalized on number of embryos per condition. Each blue dot corresponds to one embryo. Scale bar = 50µM. Error bars are shown as measure of variability and represent the standard deviation (STD). Number of biological replicates: uninjected (N=19), *pik3r1Mo* (N=29), EV+ *pik3r1Mo* (N=10), PIK3R1^{WT} + *pik3r1Mo* (N=15), PIK3R1^{N564D} (N=14), PIK3R1^{L570P} + *pik3r1Mo* (N=14), PIK3R1^{L573P} + *pik3r1Mo* (N=9). Embryos in which the CV was not readily distinguishable were discarded.

Supplementary Figure 2: Overview (10x) of zebrafish embryos at 48-54hpf. In yellow, lines indicating the angle between the head and the neck of the fish, serving as a reference for determining its developmental stage (Kimmel et al., 1955). Notably, neither morphants nor mutant fish exhibited any indication of developmental delay.

Supplementary Figure 3: Measurement of the average distance between neighboring nuclei to assess cell size. In morphant, as well as in mutant fish, cell size was significantly reduced compared to EV-injected control fish. This was not the case for overexpressing PIK3R1^{WT}, which were not significantly smaller than EV-injected fish.